universität wien

MASTERARBEIT / MASTER'S THESIS

Titel der Masterarbeit / Title of the Master's Thesis

Clay mineralogy and geochemistry of Pannonian and Sarmatian sediments from core samples in the AKH area (Vienna)

verfasst von / submitted by

Lukas Gerdenits (BSc.)

angestrebter akademischer Grad / in partial fulfilment of the requirements for the degree of

Master of Science (MSc.)

Wien, 2016/ Vienna 2016

Studienkennzahl lt. Studienblatt / degree programme code as it appears on the student record sheet:	A 066 815
Studienrichtung lt. Studienblatt / degree programme as it appears on the student record sheet:	Erdwissenschaften
Betreut von / Supervisor:	Ao. Univ. Prof. Mag. Dr. Susanne Gier

Acknowledgment

I would like to sincerely thank my supervisor Susanne Gier and Christine Jawecki, who spent a lot of time providing useful information and help for me in order to complete this thesis. Susanne Gier constantly offered her help and supported me with patience during the process of research and writing.

Christine Jawecki deserves my sincere gratitude for letting me take part in research on Miocene sediments of the Vienna Basin and giving me access to the core storage depot of the MA 29 in order to take samples of the drilling cores. She also assisted me by providing results of previous research done on the drilling cores as well as maps from the MA 29 Baugrundkataster. Last but not least I learned a lot about the current state of research by listening to her presentations.

Further I would like to thank Maria Meszar, who gave me instructions on using various scientific instruments and methods and took the time to support me whenever I needed help during my work in the laboratory.

Special thanks also go to Peter Nagl for conducting XRF spectroscopy, showing me how to prepare samples in the right way and giving me technical information about the used X-Ray spectrometer.

I also want to express my gratitude for Petra Körner, who explained me how to work on a multiphase carbon and hydrogen/moisture determinator in order to measure the total organic carbon.

I also want to thank Claudia Beybel for making thin sections of two samples.

Last but not least I am much obliged to my family who encouraged and supported me during the whole time of my study.

Index

Abstract

38 investigation wells, commissioned by the Wiener Linien GesmbH & Co KG were drilled in the urban area of Vienna in 2014. These wells were conducted by the MA 29 – Brückenbau und Grundbau for the construction of the new underground line U5, which is planned to become operational between 2025 and 2028 (Wien.at). Miocene samples of two of these wells have been investigated for this master thesis. The two wells are located north and south of the Währinger Gürtel in the area of the "Allgemeines Krankenhaus (AKH)". Well 5240 is situated north of the Währinger Gürtel on top of the Mindel-aged Arsenalterrasse, whereas well 5260 is located approximately 150 meters south-southeast on the slope to the Riss-aged Stadtterrasse.

The objectives of the study were i) to find the reasons for the colour difference (e.g. difference in clay mineralogy) between Pannonian and Sarmatian sediments, ii) to explain the difference in the thickness of the brownish weathered layers at the top of the Pannonian located right underneath the Quaternary sediments, including their depositional environment and iii) to clarify the provenance of a one meter thick cobble/sand layer, which is located at the top of the Sarmatian sediments in well 5260.

In order to compare the different sediments a variety of analytical methods have been applied. These included grainsize-analysis (wet sieving, sedimentation and Sedigraph), XRD-analysis, measurements of carbonate content and TOC, XRF-analysis and thin section microscopy.

The results did not give a clear answer to the cause of the colour difference between Pannonian and Sarmatian sediments, since XRD-analyses did not display a difference in mineralogy or clay mineralogy between the two sediment units. The difference in the thickness of the weathered sediments is caused by variations in grainsize between the two wells, as the grainsize is coarser in the upper part of the Pannonian of well 5240 compared to well 5260. This favours a better circulation of pore waters and thus a higher degree of oxidation. The brownish weathering crust is not a product of soil formation, as the CIA-value is very low and neither roots nor plant imprints could be found in the sediments, but rather relates to subaqueous alteration. This alteration either took place immediately after deposition or was caused by groundwaters afterwards, although a combination of both opportunities is also possible.

The cobble/sand layer of well 5260 contains two different types of cobbles, both of which resemble the two different types that occur in the Quaternary layers above the Miocene sediments and which have been described by Slawek (2015). Its provenance probably is the Rhenodanubic Flysch Zone and was deposited by a high energy event.

Zusammenfassung

Im Jahr 2014 wurden 38 Probebohrungen im städtischen Bereich von Wien von der Wiener Linien GesmbH & Co KG in Auftrag gegeben. Diese Bohrungen wurden von der MA 29-Brückenbau und Grundbau im Zuge der geplanten Bauarbeiten der neuen U-Bahn Linie U5 durchgeführt. Der Bau wird voraussichtlich zwischen den Jahren 2025 und 2028 abgeschlossen sein (Wien.at).

Zwei dieser im Bohrkernlager der MA 29 vorliegenden Bohrkerne wurden im Zuge dieser Arbeit untersucht, wobei nur die miozänen Sedimente Gegenstand dieser Arbeit waren. Die beiden Bohrungen liegen nördlich und südlich des Währinger Gürtels auf dem Gelände des Allgemeinens Krankenhauses (AKH). Bohrung 5240 wurde nördlich des Währinger Gürtels auf der Oberfläche der Mindel-zeitlichen Arsenalterrasse durchgeführt, während Bohrung 5260 etwa 150 Meter südsüd-östlich des Währinger Gürtels am Abhang der Arsenalterrasse zur Riß-zeitlichen Stadtterrasse stattfand.

Durch Untersuchungen miozäner Sedimente sollte unter anderem geklärt werden, welche Gründe der Farbunterschied zwischen Schichten des Pannoniums und jenen des Sarmatiums hat. In diesem Zusammenhang sollten auch etwaige Unterschiede in der Tonmineralogie ausgemacht werden. Auffällig ist die Diskrepanz in den Mächtigkeiten der verbraunten obersten Schichten des Pannoniums der beiden Bohrkerne, welche zusammen mit deren Genese auch in Bezug auf das Paläoenvironment abgeklärt werden sollte. Ein weiteres Ziel war es, die Herkunft des Materials einer etwa 1 m mächtigen Geröll- und Sandschicht am oberen Teil des Sarmatiums von Bohrkern 5260 zu eruieren.

Um die verschiedenen Schichten untereinander zu vergleichen, wurde eine Reihe von Analysemethoden angewendet, welche Korngrößenanalyse (Nasssiebung, Sedimentation und Sedigraph), XRD-Messungen, Messungen des Karbonat- und TOC-Gehaltes, XRF-Analysen und Dünnschliffmikroskopie beinhalten.

Die Resultate konnten leider keine klare Antwort auf die Frage liefern, wo der Farbunterschied zwischen Pannonium und Sarmatium herrührt, da die XRD – Messungen weder einen Unterschied in der Gesamt-, noch in der Tonmineralogie aufzeigen konnten. Die unterschiedlichen Mächtigkeiten der verbraunten Sedimente hingegen dürften jedenfalls mit den unterschiedlichen Korngrößen zusammenhängen, da gröbere Körner im obersten Pannonium des Bohrkerns 5240 im Vergleich zu jenem von Bohrkern 5260 eine bessere

Zirkulation von Porenwässern ermöglichten und daher einen höheren Oxidationsgrad bewirkten. Diese Verbraunung ist dabei nicht durch Bodenbildung entstanden, denn der CIA-Wert ist sehr niedrig, außerdem wurden weder Wurzelteile, noch Pflanzenabdrücke im Sediment gefunden. Viel eher entstand die Verbraunung durch subaquatische Alteration.

Die Geröll- und Sandschicht von Bohrkern 5260 beinhaltet zwei verschiedene Typen von Geröllen, die ebenso beide in den neogenen Sedimenten über dem Miozän vorkommen, welche von Slawek (2015) bereits eingehend beschrieben wurden. Die Herkunft dieser Gerölle, die aller Wahrscheinlichkeit nach während eines High Energy Events abgelagert wurden, dürfte wohl die Flyschzone der Ostalpen sein.

1 Introduction

The two studied wells are part of 38 investigation wells that were conducted in 2014 along the planned trail of the new underground line U5. Starting in 2018, 3 km of a new U5 track will be constructed, running from the Elterleinplatz in the 17th district of Vienna over Michelbeuern-AKH, Arne Carlsson-Park and Frankhplatz-Altes AKH to Rathaus in the first district. From there the U5 will continue on the former U2 track to Karlsplatz (Figure 1).

Figure 1: Map of the planned U5 route (source Wien.at)

The drillings were carried out to gather information about underground and groundwater conditions which will have an influence on planning the exact route and future construction work (Wien.at).

The main goal of this study was to characterize the Miocene sediments of two wells (5240 and 5260) in the area of the "Allgemeines Krankenhaus" (AKH).

Both drilling cores feature a reddish-brownish crust at the topmost part of the Pannonian, which varies greatly in thickness. Drilling core 5240 contains a 10 m thick brownish coloured sediment body, whereas in drilling core 5260 it is only 0.4 m thick. One of the objectives was

to find out why there is such a difference in thickness and whether this brownish colour is a matter of soil formation, weathering crust on the surface or subaqueous alteration.

Another aim was to figure out the reason for the colour difference between sediments of the Pannonian, which have a bluish-greyish colour, and the Sarmatian, the colour of which appears more greenish-grey. Possible reasons could for example be a difference in provenances of the sediments, the oxidation level at the seafloor, sedimentation rates or even diagenesis. For these reasons, XRD patterns were compared in order to reveal possible differences in mineralogy. TOC-value (total organic carbon) and grain-size analysis can help to disclose the state of oxidation respectively reduction, since the organic carbon content decreases in oxic environments and bigger grainsize causes higher porosity, thus a higher oxidation level.

In addition, it should be investigated if there is a difference in clay-mineralogy between sediments of the Pannonian and Sarmatian.

Last but not least an important goal was to clarify the provenance of a 0.5 m thick cobble/sand layer of core 5260, starting at 1.1 m beneath the Sarmatian-Pannonian border.

2 Geographical and geological setting

2.1 Tectonic features of the Vienna Basin

The two investigated wells are located in the 9th and 18th district in Vienna, which lies in the Vienna Basin between the Eastern Alps, Carpathian Mountains and the Pannonian Plain (Rees, 1974). The Vienna Basin is a northeast-southwest trending basin, extending into the Czech Republic and Slovakia with a northeast-southwest trend. It is approximately 200 km long and 40 km wide with a rhomboidal shape, shown in Figure 2. As a pull-apart basin it has formed along a sinistral fault system during lateral extrusion of the Eastern Alps (Royden, 1985) with a maximum sediment thickness of 5500 m. The currently existent geothermal gradient in the Vienna Basin comes to 30 °C/km (Sachsenhofer, 2001).

The evolution of the Vienna Basin can be subdivided into three major phases. The first phase corresponds to the Early Miocene during which it formed as a piggy back basin on top of thrusted and imbricated nappes of the Alpine-Carpathian fold- and thrust belt. In the second phase it evolved as a pull-apart basin from the Middle- to the Late Miocene (Decker and Peresson, 1996). Until the Early Miocene an east-west compression led to a basin inversion followed by an east-west extension from the Pleistocene until now.

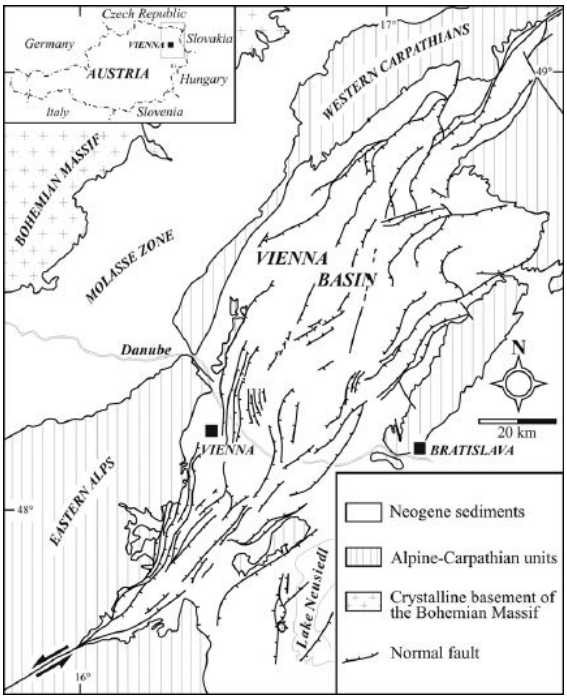

Figure 2: Location map of the Vienna Basin and surrounding areas (adapted from Wagreich and Schmid, 2002).

The Early Karpatian was characterized by a continuous filling of the Southern Vienna Basin by a huge complex of deltaic sediments. During the Late Karpatian a transgression of the Carpathian Sea flooded large parts of the Vienna Basin and lead to deposition of brackish and freshwater sediments (Kováč et al., 2004) with big rivers entering from the south. During the Badenian (Middle Miocene) fully marine conditions had already been developed in the Vienna Basin, which was connected to the Paratethys via a seaway through the Pannonian Basin (Figure 3). Sediments dated into that time correspond to marine and delta respectively slope environments alternating multiple times due to several transgression- and regression periods (Seifert, 1996). Towards the end of the Badenian or beginning of the Sarmatian the sea link between Paratethys and the Mediterranean Sea was already increasingly reduced. Consequently the salinity decreased and the alkalinity increased (Pisera, 1996). In the area of the central Paratethys the area of sedimentation was reduced, the Carpathian foreland dried out and the Pannon Sea developed in the Carpatian Arc consisting of brackish water with strongly reduced salinity (Rögl, 1999). The Pannon Sea had already turned into an extensive fresh water lake during the Pannonian (Figure 3).

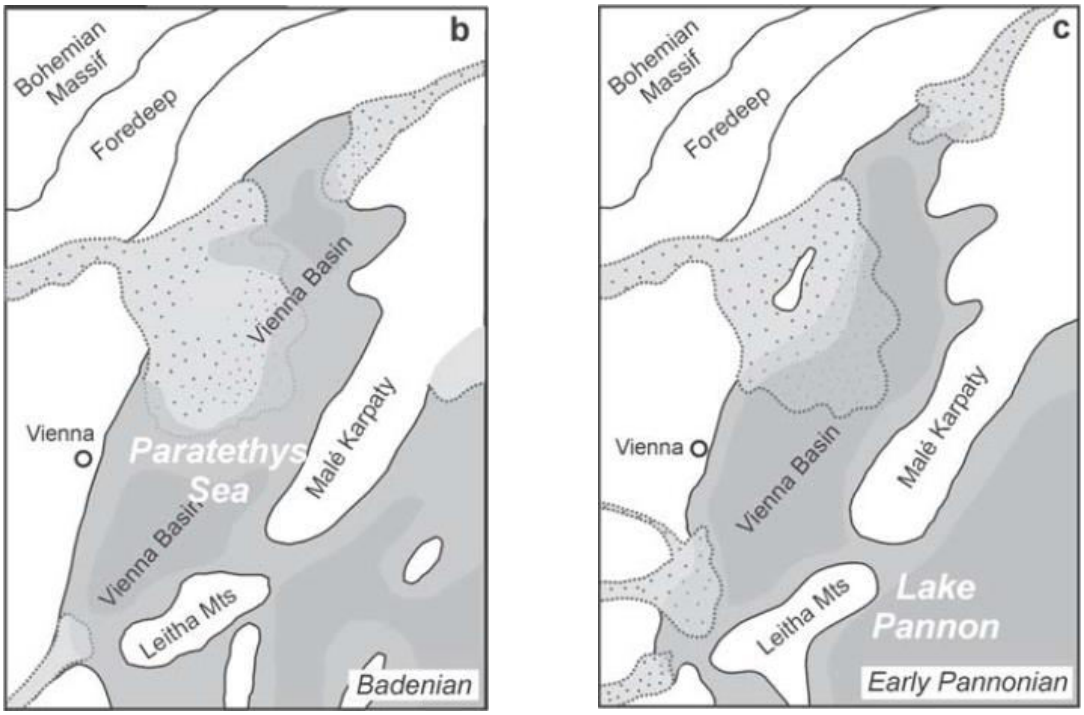

Figure 3: left: Badenian paleoenvironment of the Vienna Basin; right: Early Pannonian paleoenvironment of the Vienna Basin (Strauss et al., 2006)

2.2 Pleistocene terraces

The surface of the Vienna Basin in the area in and around Vienna is characterized by mainly five different terraces, each correlated to different ice ages in the Pleistocene. These are from the sedimentary oldest to the youngest: the Prägünz-aged Laaerbergterrasse, the Günz-aged Wienerbergterrasse, the Mindel-aged Arsenalterrasse, the Riss-aged Stadtterrasse and the Würm-aged Praterterrasse. Since the terraces have been formed by degrading melting rivers due to absence of frost debris occurring at the transition from each Glacial to Interglacial during the warm phases, the geographical highest terrace corresponds to the oldest (Reitner, 2013).

Well 5240 has been drilled on top of the Arsenalterrasse, whereas well 5260 is located approximately 50 m southeast on the estate of the AKH on top of the slope to the Stadtterrasse (Figures 4 and 5).

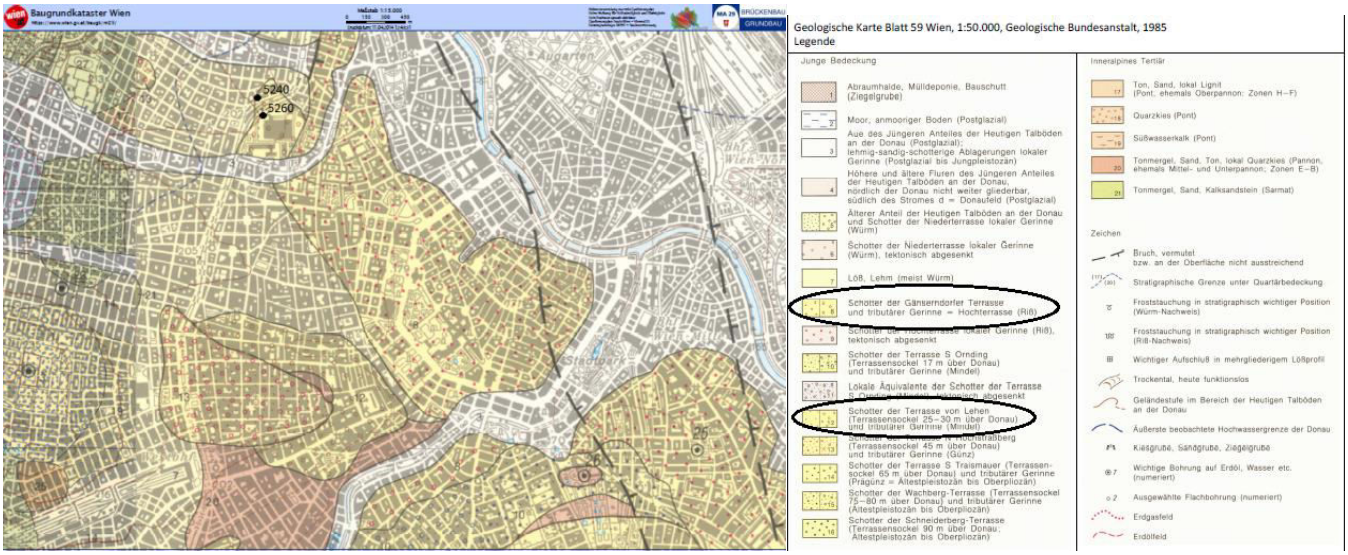

Figure 4: Exact locations of the two investigated wells 5240 and 5260 in the geological map (source ÖK 59 - MA 29 Baugrundkataster, 1:50 000)

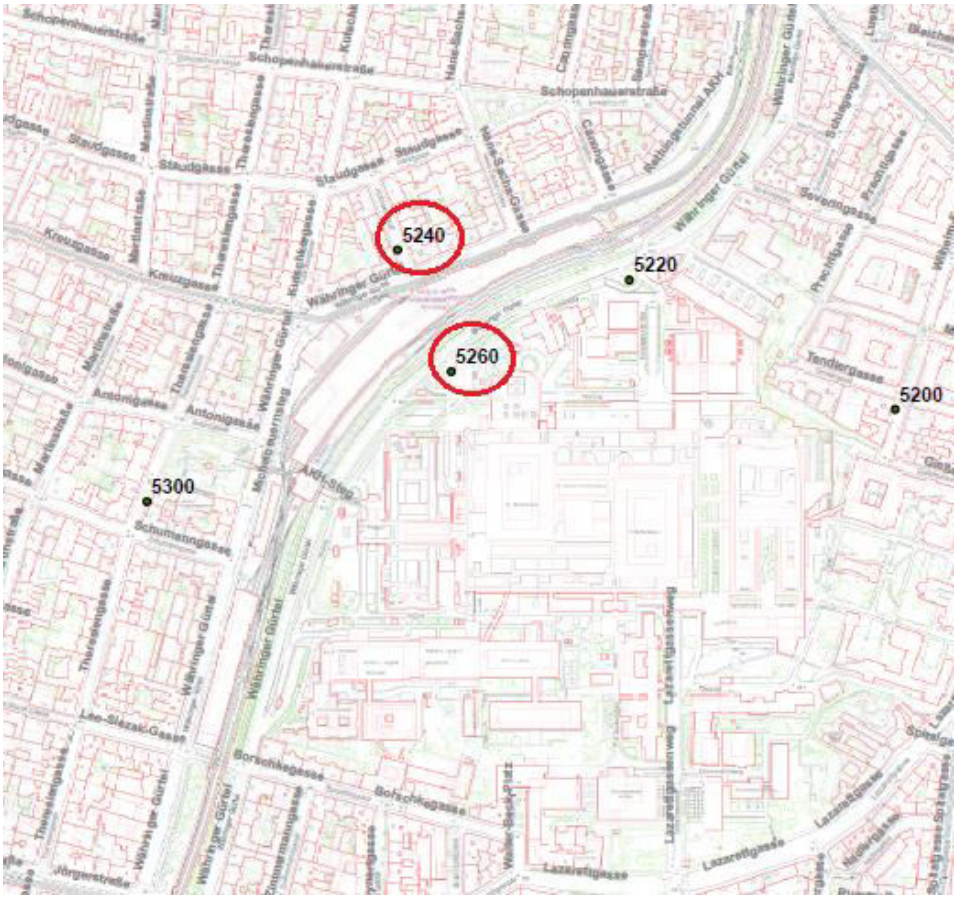

Figure 5: Exact locations of the two investigation wells 5240 and 5260 (source ÖK 59 - MA 29 Baugrundkataster, 1:50 000)

3 Materials and Methods

3.1 Core logging and Sampling

Two cores, 5240 and 5260, were logged in the core storage depot of the MA 29 (Figure 6), and altogether 17 samples of different depths were taken, which are listed in Table 1. Each layer was immediately classified according to its grainsize at first instance. The samples were taken with regard to grainsize- and colour changes throughout the succession. Afterwards they got classified in terms of colour, using the Munsell Soil Colour Chart.

Figure 6: Core boxes with sample positions (above) and sampled material (below) at the MA 29 drilling core storage

The full profiles from 16 to 60 m depth of wells 5240 (left) and 5260 (right) are shown in Figure 7.


32
33
33
34
34
35
35
36
36
37
37
38
38
39
39
40
40
41
41
42
42
43
43
44
44
45
45
46
46
47
47
48

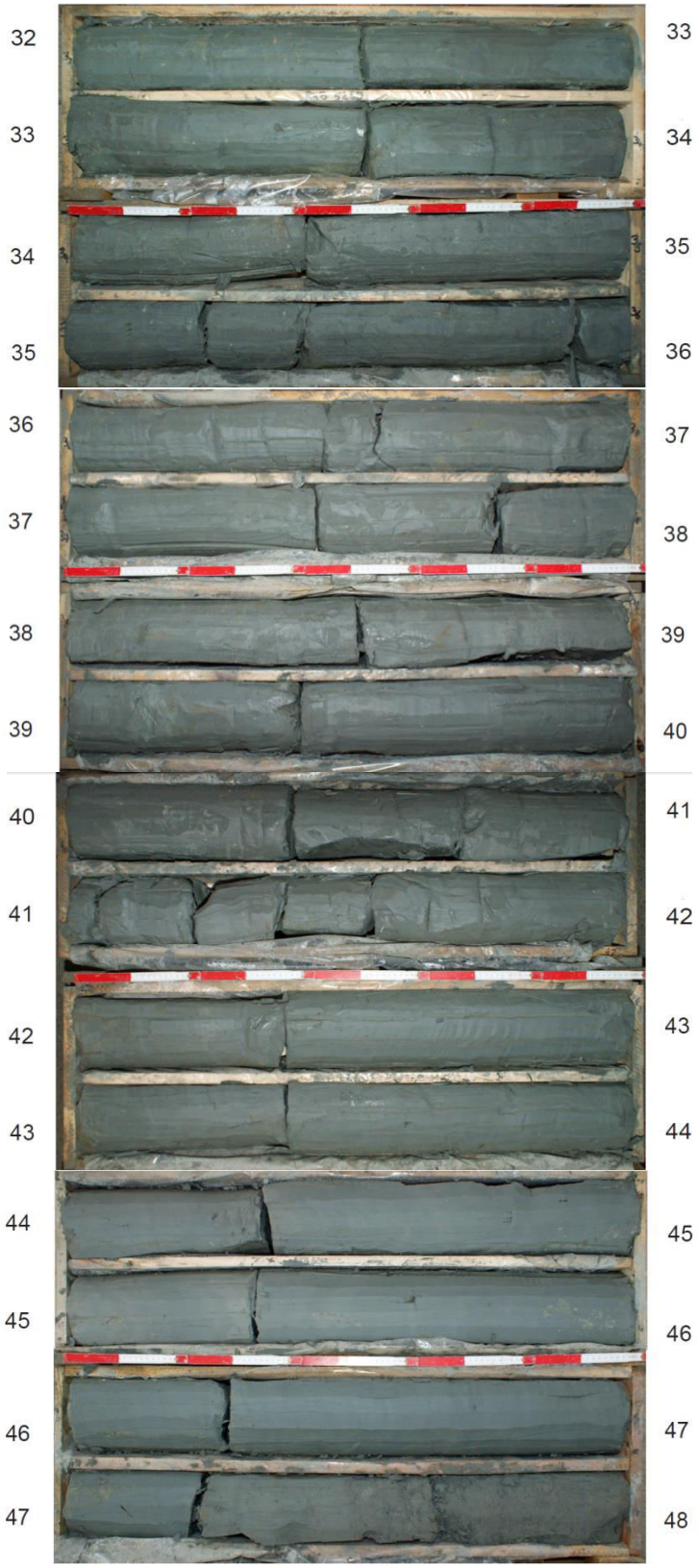
32
33
33
34
34
35
35
36
36
37
37
38
38
39
39
40
40
41
41
42
42
43
43
44
44
45
45
46
46
47
47
48

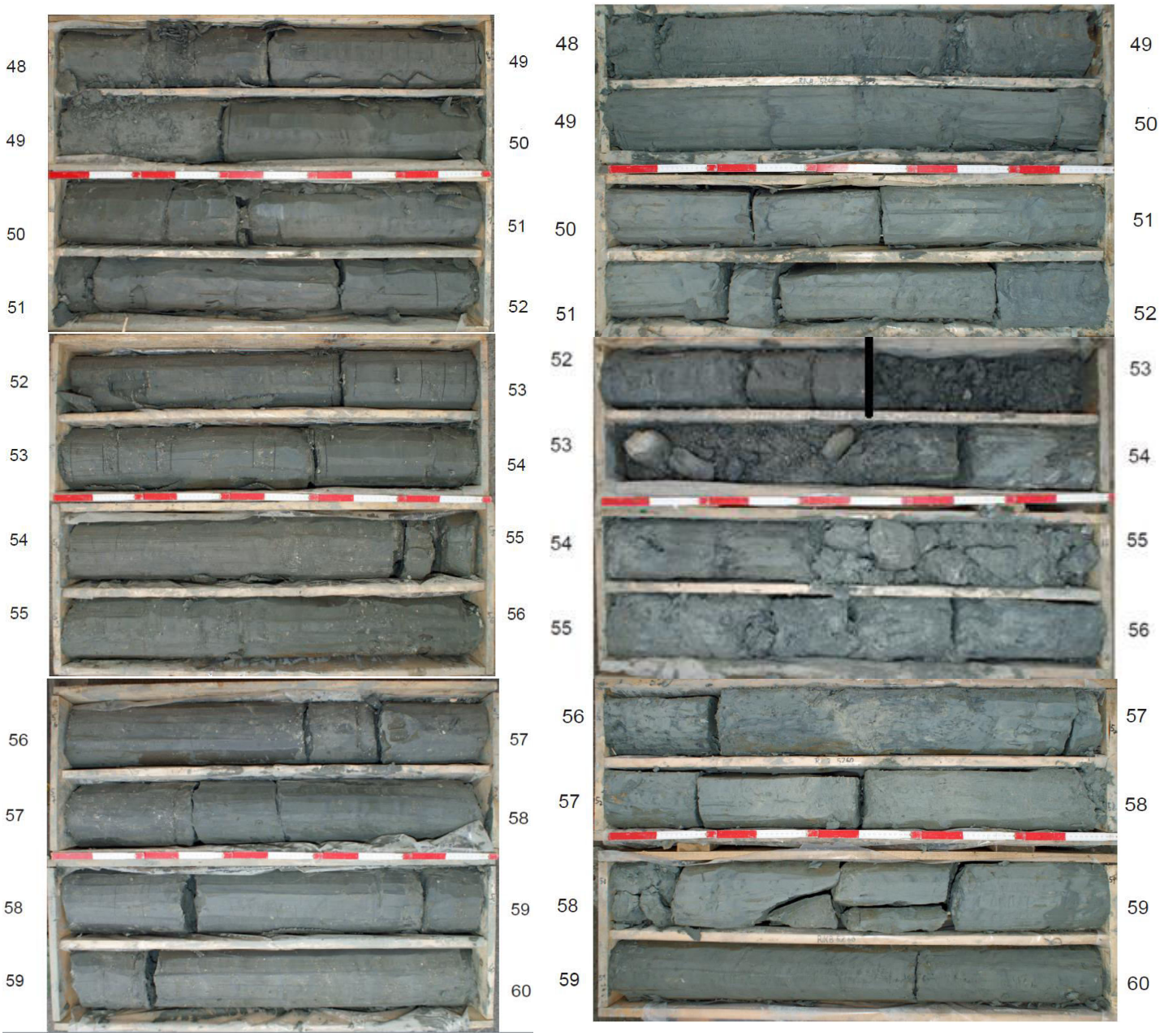

Figure 7: left: Profiles 16-60 m depth, well 5240; right: Profiles 16-60 m depth, well 5260; lithostratigraphic boundaries (Neogene - Pannonian - Sarmatian) are marked with a black line

Table 1: List of all 17 samples with their depths and stratigraphic stages

Sample Name	Depth (m)	Stratigraphic Stage
5240	18.45	Pannonian
5240	21.9	Pannonian
5240	22.6	Pannonian
5240	26.2	Pannonian
5240	33.2	Pannonian
5240	42.3	Pannonian
5240	45.6	Pannonian
5240	46.5	Sarmatian
5240	58.2	Sarmatian
5260	26.75	Pannonian
5260	32.2	Pannonian
5260	37.8	Pannonian
5260	42.4	Pannonian
5260	52.5	Pannonian
5260	53.4	Sarmatian
5260	53.9	Sarmatian
5260	59.8	Sarmatian

5240: S/P-boundary at 46.05 m

5260: S/P-boundary at 52.5 m

Note that the samples were not always taken right below or above the layer boundaries. The Sarmatian-Pannonian boundary has been defined through stratigraphic analysis by Martin Maslo, University of Vienna (personal communication).

3.2 Grain size analysis

In order to compare the grainsize distributions of the different samples, grain size analysis has been conducted, including wet sieving and measurements with a Micromeritics SediGraph 5100.

Before wet sieving the samples had to be disaggregated. Therefore 25 g of loose sample were treated with 200 ml of a mixture of H_2O_2 and H_2O (1:1) in order to oxidize the organic substances. After a week, during which the samples were stirred multiple times a day, no bubbles were rising anymore, which means that the reaction had already been finished and all the organic matter had been decomposed. Afterwards the suspensions were dispersed with an ultrasonic probe for 3 minutes at 400 W. At this point, the samples were ready for sieving using a set of sieves of 63 µm, 125 µm, 250 µm, 500 µm, 1 mm and 2 mm mesh size. After

drying each fraction in an oven at 60°C, the samples were weighed. The < 63 µm fraction was afterwards measured in a SediGraph 5100 for a detailed grain size analysis to 2 µm.
The obtained data are mass percentages in the ranges of < 2 µm, 2-4 µm, 4-8 µm, 8-16 µm, 16-31.5 µm and 31.5-63 µm.
After calculating the percentages of all grain size fractions, cumulative grain size curves and histograms could be constructed.

3.3 Chemical Analysis

For conducting a chemical analysis X-ray fluorescence spectroscopy (XRF spectroscopy) has been used.
In order to obtain the LOI (loss of ignition) approximately 3 grams of the sample powder were added to a crucible and weighed. The crucible was then placed into a muffle furnace at 850°C for a 3 hour period. After cooling it was put into a desiccator and finally weighed. The LOI was then calculated using the following formula:

LOI = [{weight(pre-ignited) - weight(ignited)} * 100] / sample weight

Sample preparation for measuring the trace elements was done by mixing 10 g of sample powder with 500 µl of polyvinyl alcohol (PVA) functioning as a binding agent. After stirring it for 10 minutes the powder could be compacted to a pressed powder pellet with 16 t/cm^2 using a pressure pump. The finished pressed powder pellet was then put into a drying oven over one night at 70 °C.
For measuring the major elements 1.2 g of this already calcined powder mixed with 6 g of $Li_2B_4O_7$ (di-lithium tetraborate) was dehydrated in an oven at 110 °C for about 12 hours and then dried in a desiccator. After 3 drops of an aqueous $LiBr_2$-solution had been added, a fused bead was produced using a PHILIPS Perl'X3 automatic bead machine. The following cycle of heating, casting and cooling completed the preparation.
After sample preparations had been finished the analyses were performed on a sequential X-Ray spectrometer Philips PW2404.

3.4 Mineralogical Analysis

Differences in mineralogy can be shown by examining samples of the two different sediment bodies using XRD (x-ray diffraction). For mineralogical analysis the dry samples were powdered in an agate bowl. In order to be fine enough for reproducible results, the grainsize had to be between 5 and 10 µm. The powdered samples were afterwards pressed with a sample stamp into a sample holder (Figure 8). Finally the XRD analysis has been conducted with a Panalytical PW 3040/60 X'Pert Pro X-ray diffractometer (CuKα radiation, 40 kV, 40 mA, step size 0.0167, 5 s per step).

Figure 8: Pressed pellets ready for XRD analysis

3.4.1 Clay Mineralogical Analysis

As clay minerals have a grain size of less than 2 µm, this fraction had to be separated from the samples. This was done using an Atterberg cylinder. First the samples were prepared in the same way as for the wet sieving process. A suspension of the dispersed sample with deionized water was filled into an Atterberg cylinder (Figure 9). Then a tip of a spatula of sodium-tripolyphosphate was added in order to prevent the fine-grained sediment from coagulation. After a sedimentation time of 24 hours and 33 minutes the 2 µm fraction could be extracted. After this time at room temperature, only the < 2 µm fraction should have remained in the water column above the deposit of the coarser grains according to Stokes Law. According to Chesworth (2008) Stokes Law is an equation that is used for determining the speed at which a spherical particle of particular size sinks in a particular medium:

$$V = \frac{2}{9} \frac{(d_p - d_1) g r^2}{\mu}$$

V represents the velocity of sinking in cm s^{-1}, d_p is the density of the sinking particles, d_1 is the density of the medium in which the particles sink down, g is the constant of gravity, r is the radius of the particles, and μ is the viscosity of the medium.

Figure 9: Sedimentation in Atterberg cylinders

After drying the suspension in a drying oven at 40°C the remaining clay got powdered in an agate bowl.

Clay minerals are generally hard to distinguish with x-ray diffraction (XRD), since their peaks often plot at d-values that interfere with each other. Furthermore inhomogeneous cation occupations and hydration conditions can lead to undefined basic reflexes when it comes to expandable structures. Hence interlayers have to be occupied by organic molecules or special cations (e.g. K, Mg) in order to reach homogeneous widening structures (Jasmund and Lagaly, 1993). The resulting five patterns for every sample definitely display the contained clay-minerals and may reveal a possible difference between the sediments of the Pannonian and Sarmatian.

Of each sample two portions of 50 mg of fine powder got weighed in. One portion was saturated with $MgCl_2$ and the other one with KCl, both inside test tubes of 50 ml. Then all samples were rotated overhead for about 24 hours and afterwards centrifuged for 5 minutes at a rate of 1500 spins per minute. After pouring away the salt solutions, the test tubes were

filled again with distilled water and dispersed. After this they were centrifuged again, this time for 10 minutes at a rate of 4000 spins per minute. After taking them out and pouring the liquid away again the remaining sample got mixed with 5 ml of distilled water. Then the samples got dispersed inside the test tubes with an ultrasonic probe. Two portions of 1 ml of the K- saturated sample (10 mg sample/ml) were pipetted onto two small glass slides and one portion of 1 ml of the Mg-saturated sample onto one glass slide. After this all glass plates were air-dried.
The identification of the clay minerals with x-ray diffraction is generally done by using their basal reflections (d_{001}). Oriented preparations in which the layers of the sheets (morphological (001) – layers) are orientated parallel to the object carrier plain ensure that the 001-reflexes appear more strongly (Jasmund and Lagaly, 1993).

The K-exchanged samples additionally got saturated with ethylene glycol, while the Mg-samples were saturated with glycerol. The second K-saturated sample was heated to 550 °C.
Saturating the samples with ethylene glycol and glycerol causes some swellable clay minerals to widen the distances between their lattice plains. Smectite for example expands the space between its lattice planes when saturated with Mg and glycerol or K and ethylene glycol, so that the peak changes to 18 Å respectively 17 Å, whereas vermiculite, which is another swellable mineral, does not. When vermiculite gets saturated with K^+-ions and/or heated to 300 °C, its main peaks change from 14 Å to 10 Å, whereas the peak of chlorite stays at 14 Å when experiencing the same conditions.

3.4.2 Estimating Mineral Quantities by Peak intensities

Although the mineralogical analysis was only of qualitative value, an attempt has been made to estimate their relative quantity. By comparing the peak intensities one can quite precisely point out the difference in abundance of different minerals between the samples. For this estimation the samples all have to be prepared the same way.

3.5 Total Organic Carbon Measurement

In order to measure the total organic carbon (TOC) 150 mg of finely ground sample was placed into the measuring cell of a Leco RC612. A pipeline connected to the cell filled it with O_2. The sample was heated to 550 °C in order to vaporize and oxidize the organic carbon. The resulting gas was led into a catalyser to make sure that every other gas originated from the carbon (e.g. CO) turned to CO_2. The amount of CO_2 was then measured by an infrared detector. The machine automatically calculated the TOC content out of the measured amount of CO_2. Each measurement took about 20 minutes.

3.6 Carbonate Measurement

Figure 10: Karbonat-Bombe by Müller and Gastner (1971)

For measuring the carbonate content of the samples a "Karbonat-Bombe" by Müller and Gastner (1971) has been used (Figure 10). Approximately 0.60 g of the pulverized samples was weighed in inside a plexi-glass cylinder. Then a small amount of 25% HCl was poured to the measuring line of a small plastic container that is attached to the bottom side of the cap. After screwing the cap onto the glass cylinder the whole device was turned overhead in order to pour the HCl onto the sample powder. A manometer calibrated in % $CaCO_3$ attached to the upper side of the cap then measured the pressure change that occurred due to the formation of CO_2 by carbonate dissolution (Müller and Gastner, 1971).

Chemical equation of the reaction: $CaCO_3(s) + 2\ HCl(aq) = H_2O(l) + CO_2(g) + CaCl_2(aq)$

After 15 minutes during which the “Karbonat-Bombe” had been shaken several times the reaction could be seen as completed and the final carbonate value could be read. All the samples were measured twice in order to assure the correctness of the results.

4 Results

4.1 Lithostratigraphy

The sedimentary sequences of both drilling cores are shown in the two lithostratigraphic logs below (Figures 11 + 12). The stratification consists of alternating argillaceous mudstones, but also some siltstones, sandy layers and a 1 m thick cobble/sand layer in well 5260. The two logged profiles reach from 16.2 m – 60 m (43.8 m length) in the case of well 5240 and from 20.4 m – 60 m (39.6 m length) for well 5260.

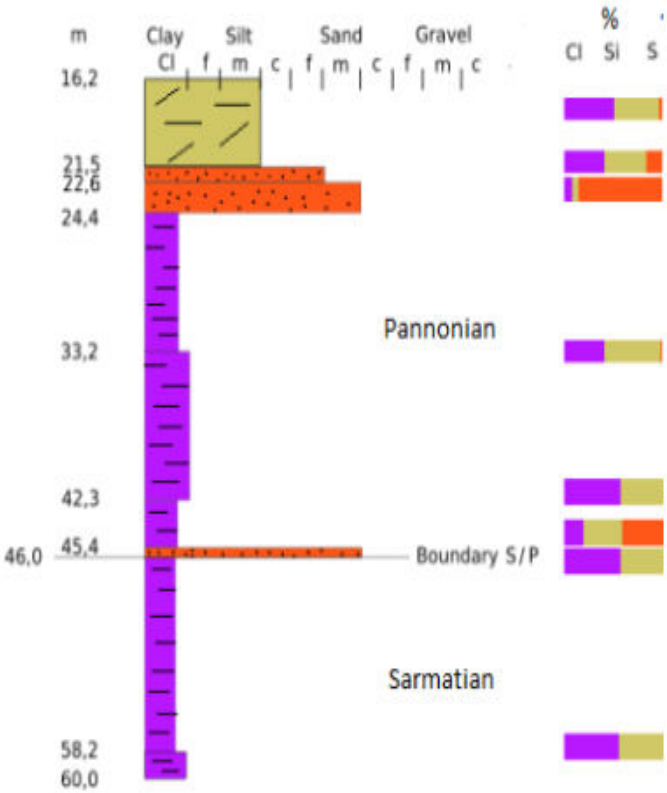

	Core 5240	
Depth (m)	Estimated Grainsize and fossil content	Munsell Soil Colour Code
16.2 – 21.5	Silt, no fossils	Light olive brown 5Y 5/6
21.5 – 22.6	Fine sand, no fossils	Dark yellowish orange 10YR 6/6
22.6 – 24.4	Medium sand, no fossils	Moderate brown 5YR 3/4
24.4 – 32.2	Clayey Silt, low fossil content	Greenish gray 5GY 6/1
33.2 – 42.3	Clay, low fossil content	Olive gray 5Y 4/1 to Light olive gray 5Y 6/1
42.3 – 45.4	Clay, no fossils	Olive gray 5Y 4/1
45,4 – 46.0	Sand, no fossils	Greenish gray 5GY 6/1 to Olive Gray 5Y 4/1
46.0 – 58.2	Clay, high fossil content	Greenish gray 5G 6/1
58.2 – 60.0	Clay, very high fossil content	Greenish gray 5GY 6/1 to Dark greenish gray 5GY 4/1

Figure 11: Lithostratigraphic profile of well 5240 (Pannonian and Sarmatian)

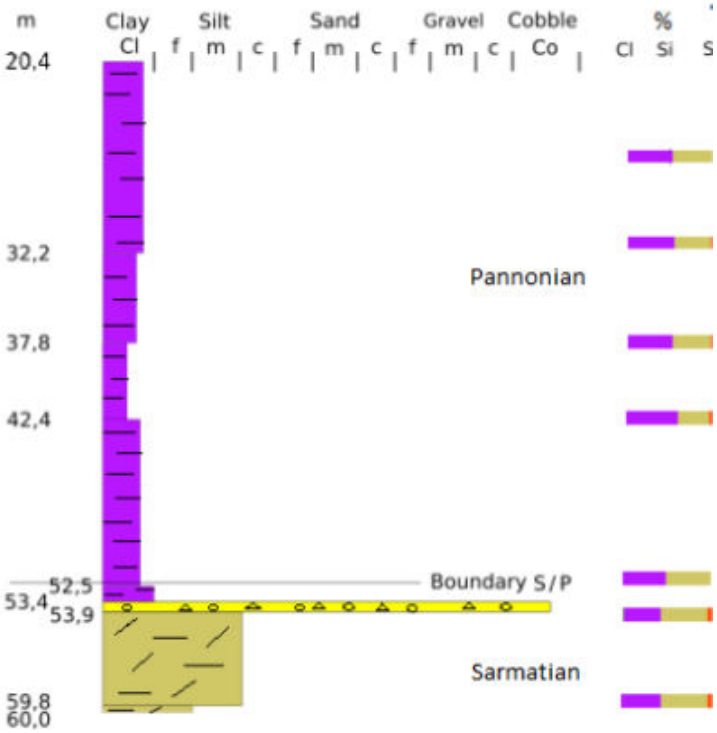

	Core 5260	
Depth (m)	Estimated Grainsize and fossil content	Munsell Soil Colour Code
20.4 – 32.2	Clay, no fossils	Greenish gray 5GY 6/1
32.2 – 37.8	Clay, low fossil content	Greenish gray 5GY 6/1
37.8 – 42.4	Clay, no fossils	Dark greenish gray 5GY 4/1
42.4 – 52.5	Clay, no fossils	Olive gray 5Y 4/1
52.5 – 53.4	Clay, low fossil content	Dark greenish gray 5GY 4/1
53.4 – 53.9	Cobble, no fossils	
53.9 – 59.8	Silt, no fossils	Pale olive 10Y 6/2
59.8 – 60.0	Clayey Silt, very high fossil content	Dark greenish gray 5GY 4/1

Figure 12: Lithostratigraphic profile of well 5260 (Pannonian and Sarmatian)

4.2 Grain size Distribution

Most of the samples have a clay content between 50 and 60 % (see Table 2), which classifies them as silty clays. Figure 14 shows cumulative grain size curves for well 5260, which reveal similar grain size distributions for all samples. The deepest three samples have silt contents of over 50 %, which is higher than the other samples featuring contents of between 36 and 45 %. On the other hand the deeper samples display a lower clay content of 40 – 47 % in respect to the 54 – 58 % clay content of the upper ones. Most sand contents are around 1 %, except for samples 5260-42,4, 5260-53,9 and 5260-59,8. The sand contents of these three samples are between 5 and 7.5 %.

Some samples of well 5240 are coarser grained then the others, namely 5240-22,6 and 5240-45,6, which mainly consist of sand. 5240-21,9 is the only sample that contains 13.5 % very fine gravel and 4.5 % sand. The rest of the samples in well 5240 have clay and silt contents varying between 40 and 60 % and sand contents below 2 % (Figure 13).

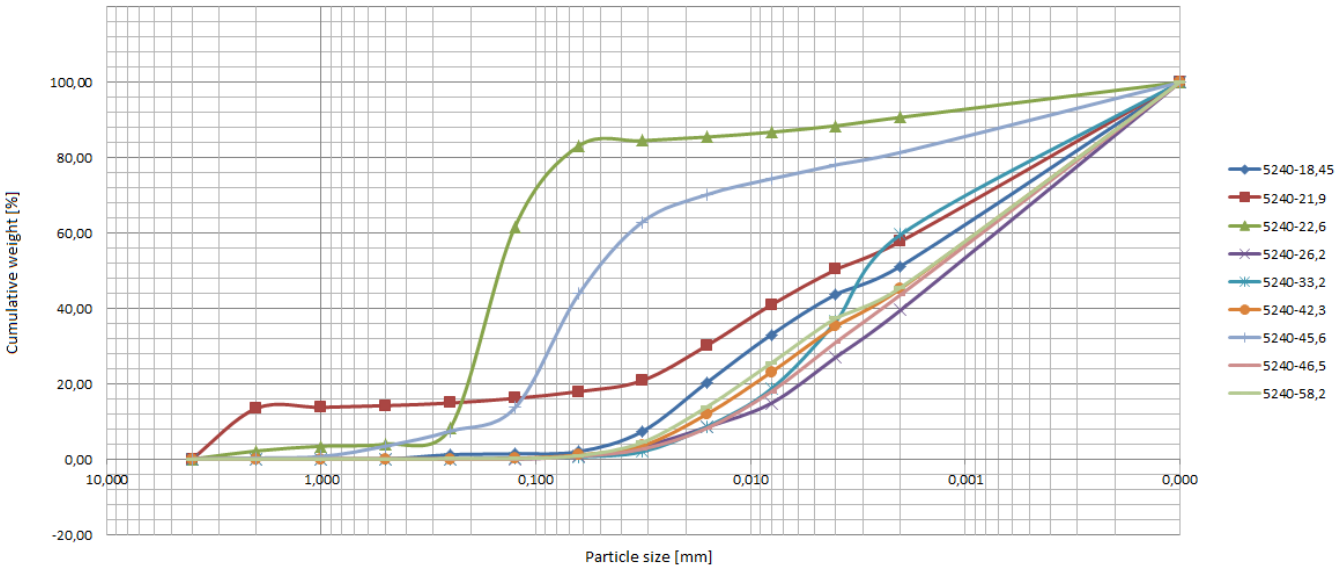

Figure 13: Cumulative grain size curves for samples of well 5240

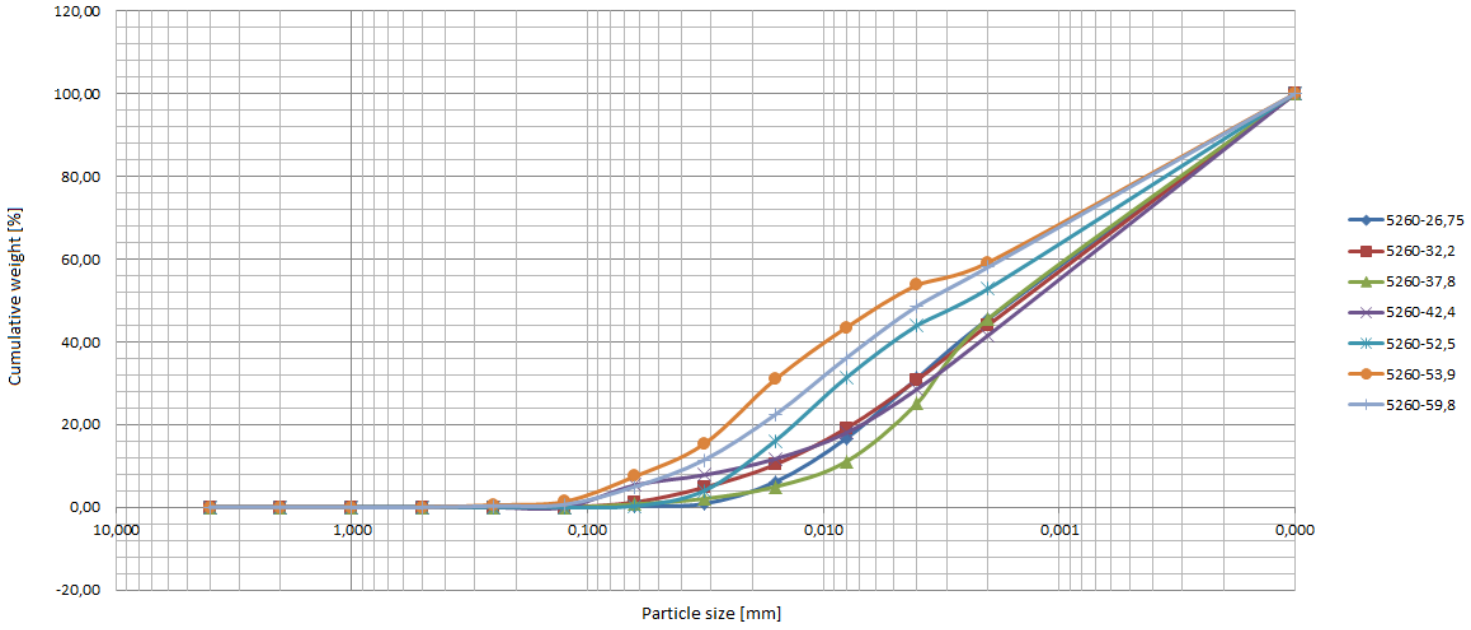

Figure 14: Cumulative grain size curves for samples of well 5260

Table 2: Grain size distribution of all samples

Sample	Clay [%]	Silt [%]	Sand [%]
5240-18,45	48.81	49.20	1.99
5240-21,9	42.22	39.84	17.93
5240-22,6	9.28	7.58	83.14
5240-26,2	60.48	38.67	0.85
5240-33,2	40.43	58.96	0.61
5240-42,3	54.78	44.10	1.12
5240-45,6	18.59	37.56	43.85
5240-46,5	56.38	42.88	0.74
5240-58,2	54.49	44.58	0.92
5260-26,75	54.49	45.15	0.36
5260-32,2	55.94	42.82	1.24
5260-37,8	54.41	44.82	0.78
5260-42,4	58.42	36.23	5.35
5260-52,5	47.15	52.54	0.31
5260-53,9	40.80	51.74	7.47
5260-59,8	41.94	53.07	4.99

Since the classification of mudstones by mineralogy is somehow problematic because of the difficulty in yielding quantitative data due to very small grainsize, they can better be subdivided after their grainsize (Boggs, 2006). The examined samples are therefore plotted into the classification diagram after Picard (1971) in Figures 15 and 16. Most samples of both wells can be classified as silty clays and clayey silts, the latter possessing a slightly higher silt- than clay content. Only sample 5240-45,6 plots in the area of sandy mud, 5240-21,9 and 5240-33,2 in the area of clayey mud and sample 5240-22,6 can clearly be classified as sand.

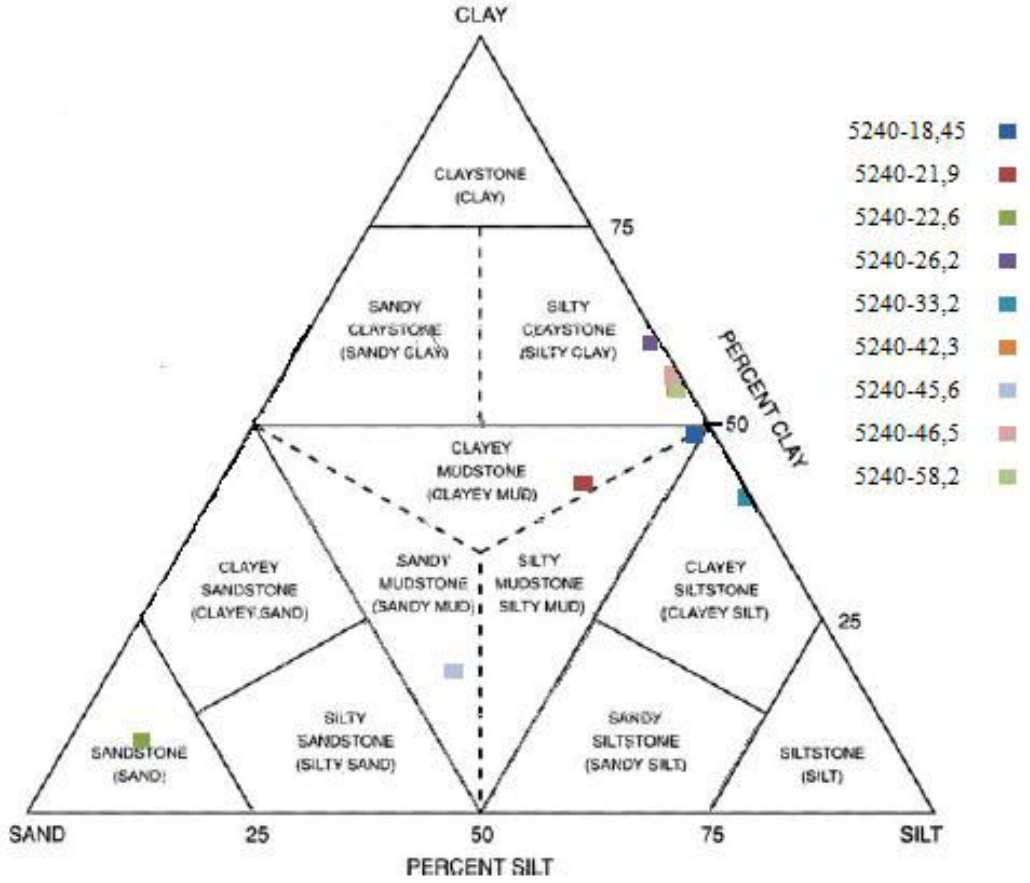

Figure 15: Textural classification of samples after Picard (1971) for well 5240

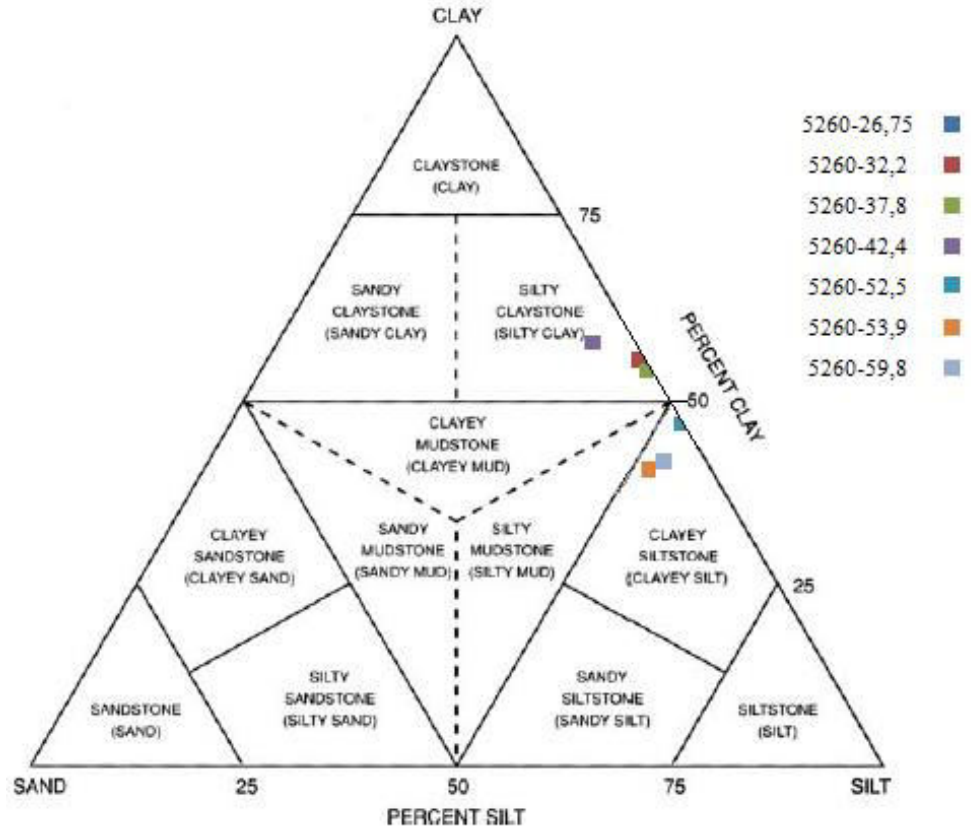

Figure 16: Ternary diagram of textural classification of samples after Picard (1971) for well 5260

4.3 Chemical Analysis and Chemical Index of Alteration (CIA)

Chemical analyses were carried out on all samples, the results are listed in Table 3.

Table 3: Table showing the chemical data obtained from XRF analysis

Sample	5240-18,45	5240-21,9	5240-22,6	5240-26,2	5240-33,2	5240-42,3	5240-45,6	5240-46,5	5240-58,2
Compound Name	Conc. [%]	Conc. [%]	Conc. [%]	Conc. [%]	Conc. [%]	Conc. [%]	Conc. [%]	Conc. [%]	Conc. [%]
SiO_2	56.000	56.000	59.000	49.000	49.000	54.000	63.000	49.000	51.000
TiO_2	0.810	0.840	0.290	0.770	0.770	0.670	0.610	0.700	0.740
Al_2O_3	18.000	18.000	5.000	17.000	18.000	12.000	8.300	16.000	17.000
Fe_2O_3(total)	6.900	8.900	4.500	5.900	6.700	3.900	2.700	4.900	5.000
MnO	0.130	0.140	0.120	0.071	0.089	0.062	0.060	0.110	0.091
MgO	2.200	2.100	0.520	3.100	3.300	2.400	1.600	3.300	2.600
CaO	4.800	2.800	5.000	8.000	6.100	11.000	12.000	9.300	7.200
Na_2O	0.710	0.670	0.630	0.570	0.580	1.000	1.000	0.580	0.690
K_2O	3.200	3.300	1.100	3.300	3.300	2.200	1.800	3.200	3.200
P_2O_5	0.120	0.150	0.190	1.000	0.120	0.110	0.120	0.084	0.076
sum	92.870	92.900	76.350	88.711	87.959	87.342	91.190	87.174	87.597
LOI(1050°)	7.260	6.230	23.190	10.710	11.420	10.740	7.000	12.750	10.750
F				0.170	0.130				0.091
SO_3	0.019	0.011	0.022	0.028	0.700	1.500	1.100	0.088	1.400
Cl	0.010	0.008	0.014		0.005	0.008	0.010	0.008	0.005
total	100.159	99.149	99.576	99.619	100.214	99.590	99.300	100.020	99.843
Sc									
V									
Cr	0.014	0.016	0.012	0.018	0.016	0.011	0.015	0.014	0.014
Co		0.011	0.007	0.006				0.007	0.008
Ni	0.014	0.015	0.010	0.015	0.016	0.011	0.014	0.013	0.014
Cu	0.007	0.005	0.002	0.009	0.006	0.006	0.002	0.005	0.005
Zn	0.012	0.011	0.003	0.010	0.012	0.007	0.005	0.012	0.010
Ga	0.002	0.002		0.002	0.002			0.002	0.002
As	0.004	0.004	0.004			0.002	0.007		
Rb	0.030	0.033	0.003	0.043	0.029	0.030	0.006	0.025	0.031
Sr	0.015	0.014	0.008	0.022	0.018	0.029	0.034	0.020	0.022
Y	0.006	0.006	0.003	0.007	0.006	0.004	0.005	0.006	0.005
Zr	0.027	0.026	0.048	0.020	0.019	0.035	0.100	0.019	0.020
Nb	0.002	0.002		0.002	0.001	0.001		0.002	0.001
Ba	0.050	0.057	0.024	0.039	0.043	0.032	0.030	0.033	0.033
La									
Ce				0.016	0.032	0.018	0.016	0.021	0.020
W	0.005		0.008	0.010	0.009		0.012	0.012	0.006
Pb	0.003	0.005		0.004	0.005	0.004	0.002	0.005	0.004
Th		0.002			0.002				

Sample	5260-26,5	5260-32,2	5260-37,8	5260-42,40	5260-52,5	5260-53,9	5260-59,8
Compound Name	Conc. [%]	Conc. [%]	Conc. [%]	Conc. [%]	Conc. [%]	Conc. [%]	Conc. [%]
SiO_2	53.000	54.000	49.000	51.000	54.000	57.000	49.000
TiO_2	0.820	0.790	0.750	0.770	0.730	0.740	0.670
Al_2O_3	17.000	18.000	18.000	18.000	14.000	15.000	14.000
Fe_2O_3(total)	6.500	5.700	7.000	6.000	4.300	3.600	4.500
MnO	0.074	0.069	0.095	0.063	0.060	0.170	0.210
MgO	3.100	3.000	3.300	3.400	2.500	2.200	2.800
CaO	5.300	4.900	5.800	5.500	9.100	8.500	11.000
Na_2O	0.770	0.650	0.620	0.560	0.900	0.900	0.780
K_2O	3.200	3.300	3.200	3.300	2.700	2.900	2.600
P_2O_5	0.110	0.095	0.110	0.100	0.160	0.120	0.140
sum	89.874	90.504	87.875	88.693	88.450	91.130	85.700
LOI(1050°)	9.570	8.760	11.480	10.850	9.800	8.710	11.470
F		0.120	0.160	0.110	0.120	0.100	0.100
SO_3	0.035	0.100	0.690	0.590	1.500	0.300	2.300
Cl	0.005			0.005	0.011	0.009	0.007
total	99.484	99.484	100.205	100.248	99.881	100.249	99.577
Sc							
V							
Cr	0.015	0.014	0.015	0.017	0.009	0.010	0.012
Co	0.008		0.009	0.007	0.007		0.006
Ni	0.015	0.012	0.017	0.014	0.011	0.012	0.014
Cu	0.005	0.006	0.004	0.004	0.005	0.015	0.003
Zn	0.012	0.012	0.011	0.012	0.007	0.008	0.009
Ga	0.002	0.002	0.002	0.002	0.001	0.002	0.001
As				0.003			0.004
Rb	0.028	0.030	0.015	0.034	0.033	0.029	0.022
Sr	0.014	0.016	0.019	0.018	0.023	0.024	0.032
Y	0.006	0.007	0.006	0.006	0.006	0.005	0.005
Zr	0.025	0.024	0.018	0.019	0.030	0.032	0.031
Nb	0.002	0.002	0.002	0.001	0.001	0.002	0.001
Ba	0.042	0.036	0.041	0.041	0.031	0.035	0.031
La							
Ce	0.026	0.026	0.028	0.024	0.030	0.033	0.016
W	0.006	0.009			0.010	0.013	0.009
Pb	0.004	0.004	0.005	0.005	0.005	0.003	0.002
Th	0.002					0.002	

The data in table 2 show the values of the most important major-, minor- and trace elements as well as the LOI of each sample. SiO_2 values vary between 49 and 63 %, most being close to 50 %. The coarser grained samples 5240-22,6 and 5240-45,6 have the lowest Al_2O_3 value. Fe_2O_3 contents vary between 2.7 – 8.9 %, whereas the reddish samples do not have significant higher values. Sample 5240 has a relatively low MgO content of 0.5 % compared to the others (1.6 – 3.4 %).

The Chemical Index of Alteration (CIA) is the most widely used index for describing the degree of chemical weathering in sedimentary detritus (Potter, 2005) and can also give a hand in reconstructing paleo climate conditions:

$$CIA = \left(\frac{Al_2O_3}{Al_2O_3 + Na_2O + K_2O + CaO^*}\right) \bullet 100$$

In order to get rid of the effects of high carbonate contents, which can distort the chemical index of alteration, one can rewrite the equation without using CaO (Nesbitt and Young, 1982). The adapted formula is:

$CIA = Al_2O_3/(Al_2O_3+Na_2O+K_2O)*100$

Figure 17 shows the CIA value including CaO with depth, Figure 18 excluding CaO. Samples of well 5260 have much more constant CIA values with depth than those from well 5240. They vary between 79 and 83% with relatively higher values in the upper samples. On the contrary two samples of drilling core 5240 (22.6 m and 45.6 m) possess a significantly lower CIA value, both mostly consisting of sand. These are sample 5240-22,6 containing reddish sand and located in the brownish area of the upper Pannonian and sample 5240-45,6 consisting of greenish-gray sand that does not differ from the samples taken above or below in terms of colour.

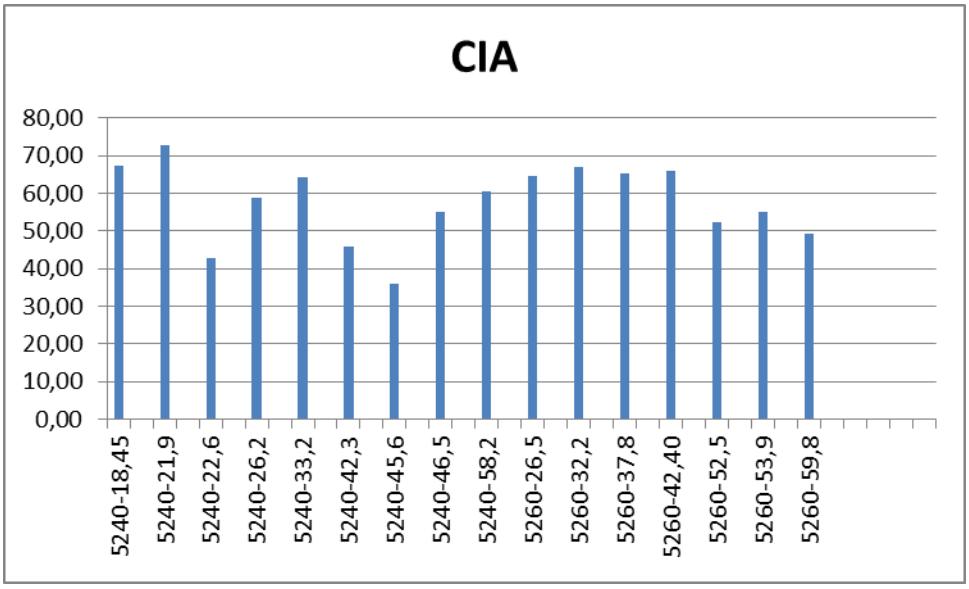

Figure 17: CIA values with depth

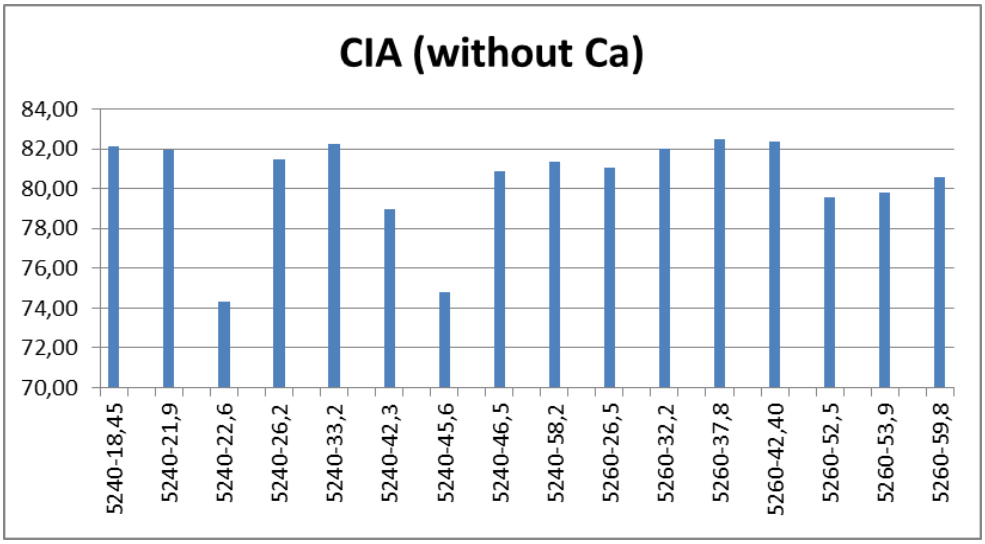

Figure 18: CIA values with depth without considering CaO

The content of Al_2O_3 and TiO_2 in mudstones is important, since these highly resistant oxides are hardly affected by weathering and diagenesis as a consequence of their insolubility in most pore fluids (Andersson and Worden, 2004).

These features are required in order to highlight a possible change in provenance. The absolute contents of either Al_2O_3 or TiO_2 are not very representative, because they are strongly affected by dilution of minerals like quartz, calcite or dolomite. Therefore a ratio between the two oxides was used (Figure 19).

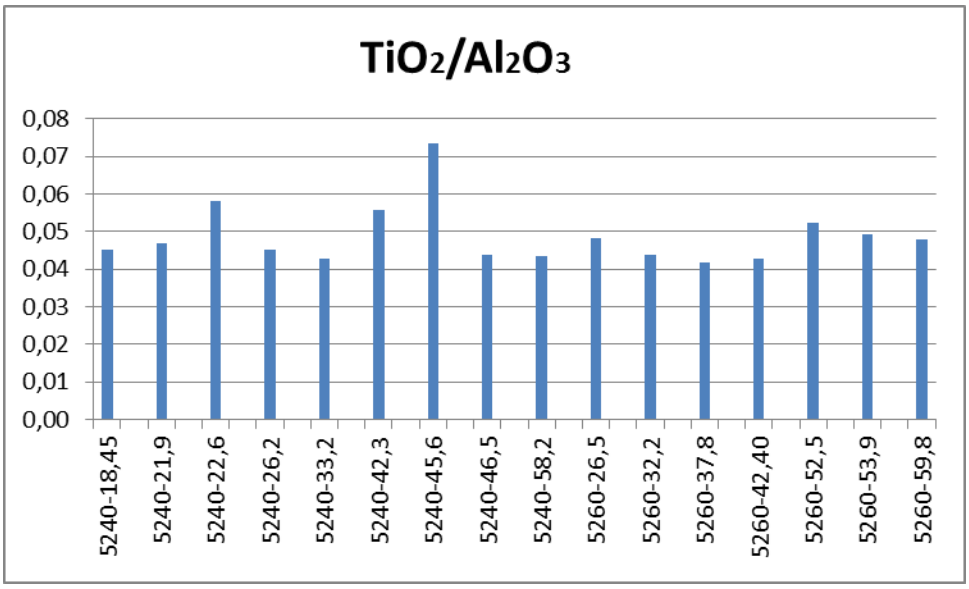

Figure 19: Ratio between TiO_2 and Al_2O_3

According to Boggs (2006), the content of magnesium in mudstones is predominantly controlled by clay minerals, but some magnesium is also incorporated in dolomite and biotite. The abundance of these two minerals is therefore also to some extent representative for the total content of magnesium in the samples (Figure 20).

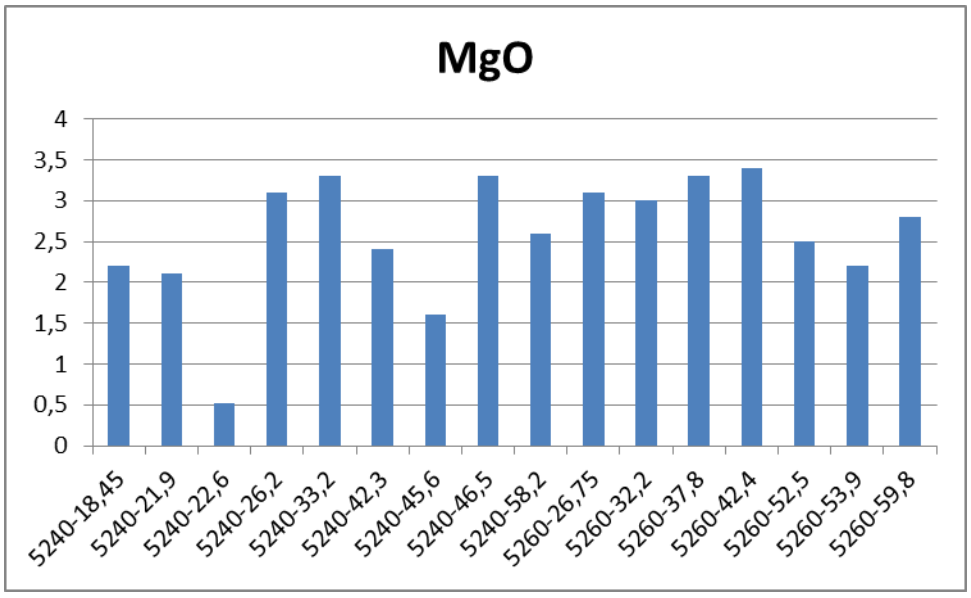

Figure 20: Content of MgO

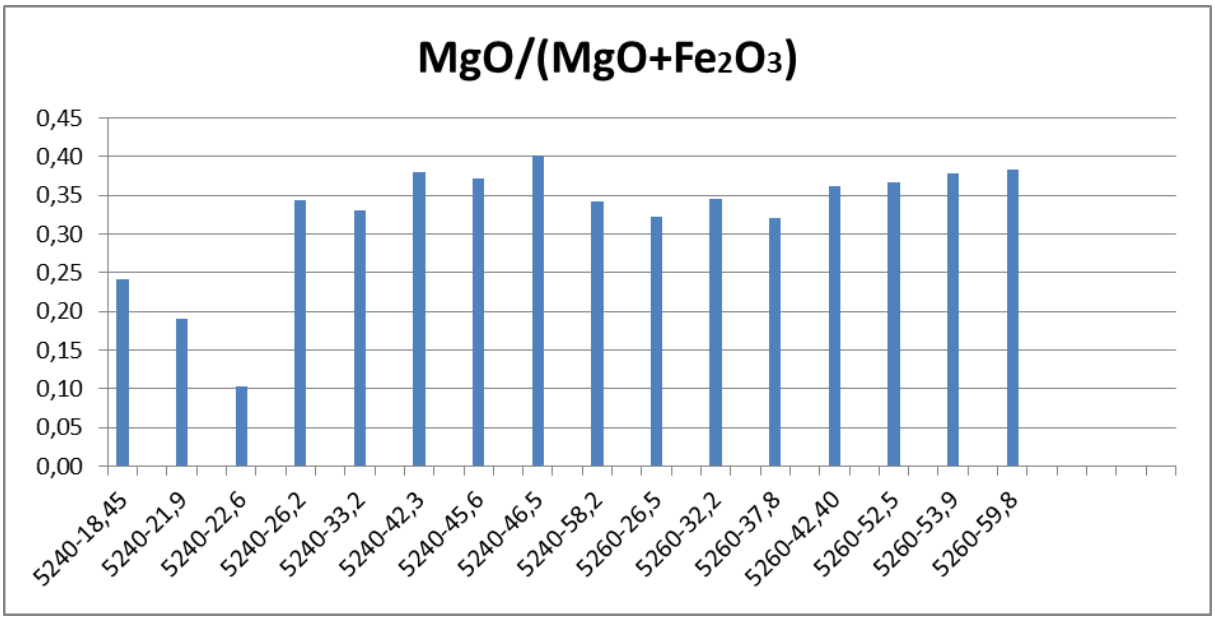

Figure 21: Ratio between MgO and Fe_2O_3

The ratio between MgO and Fe_2O_3 generally stays quite constant between 0.32 and 0.40. The upper three brownish and reddish samples of well 5240 have much lower MgO/(MgO+Fe_2O_3) – ratios (Figure 21).

The abundance of SO_3 (Figure 22) is also very strongly connected to the presence of pyrite, which means that most sulfur is incorporated into pyrite.

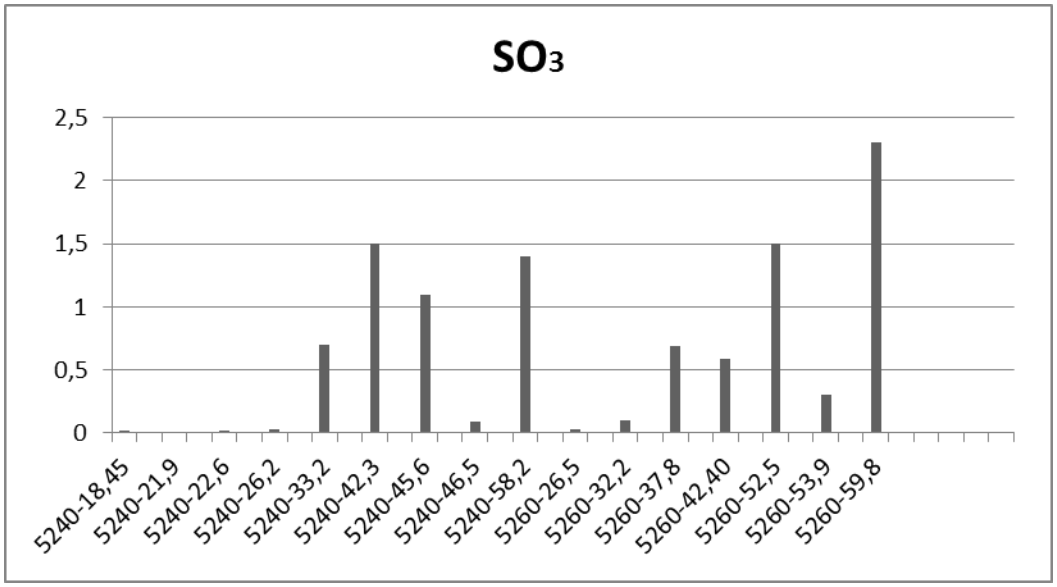

Figure 22: Content of SO_3

4.4 Mineralogy

The X-ray patterns of all the bulk samples are very similar, Figure 23 shows a pattern representative for all other samples. The following minerals could be detected throughout the samples: Quartz, calcite, K-feldspar, plagioclase and muscovite. In some also dolomite, biotite and pyrite were found. The differentiation of clay minerals like smectite, chlorite, vermiculite, illite and kaolinite in the bulk samples is somewhat problematic, hence further sample preparation is mandatory to properly distinguish those minerals.

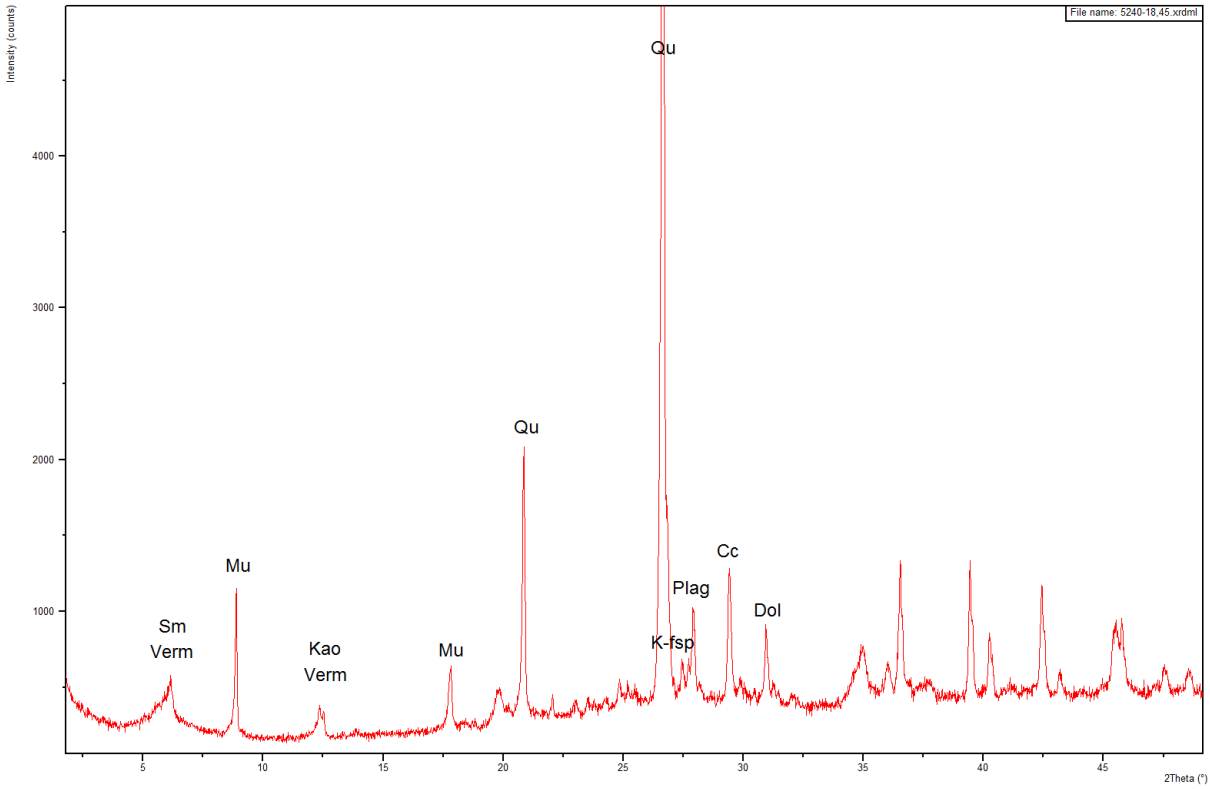

Figure 23: X-ray pattern of bulk sample 5240-18,45 m

The XRD patterns of the clay minerals are also very similar to each other. Minerals detected were smectite (montmorillonite), vermiculite, illite, kaolinite and traces of chlorite, presumably clinochlore. All these minerals were found in every single sample examined. Figures 24 and 25 show representative clay mineral patterns of Pannonian (5240-42,3) and Sarmatian (5240-46,5) samples.

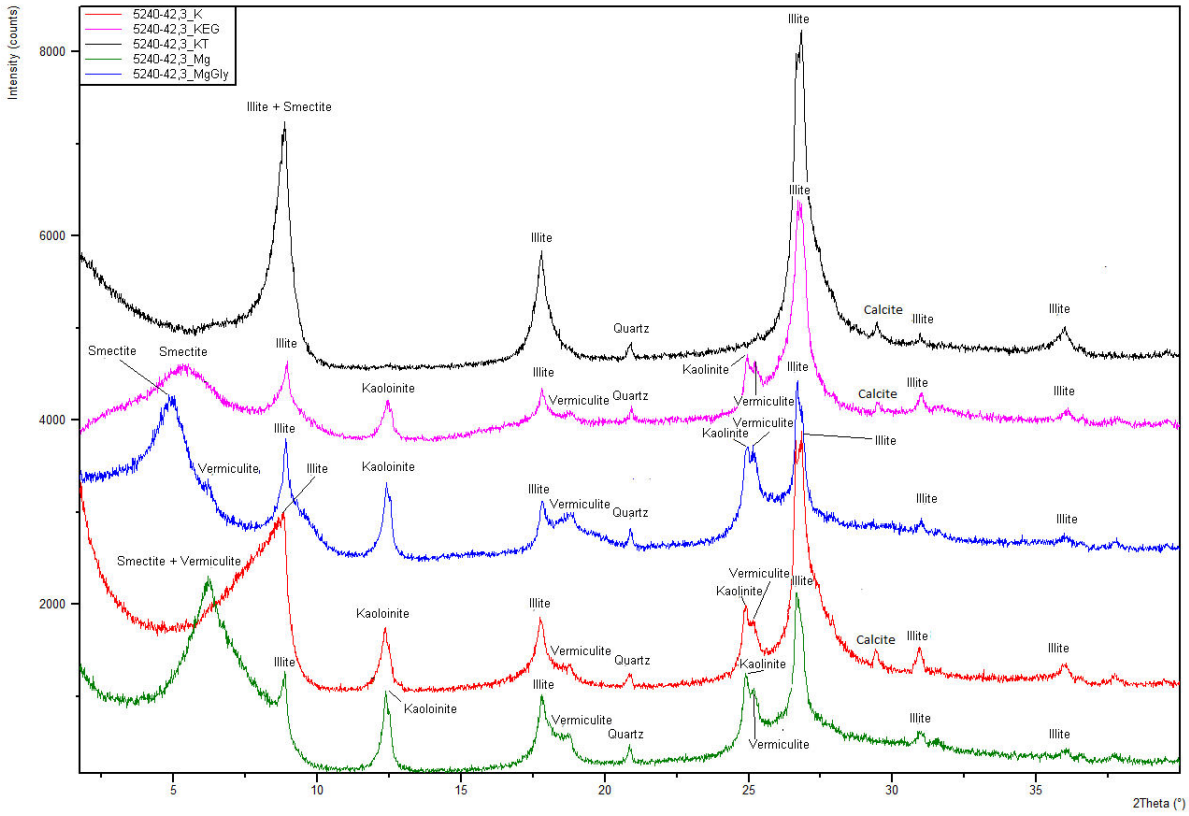

Figure 24: XRD patterns showing the clay mineralogy of sample 5240-42,3; Pannonian

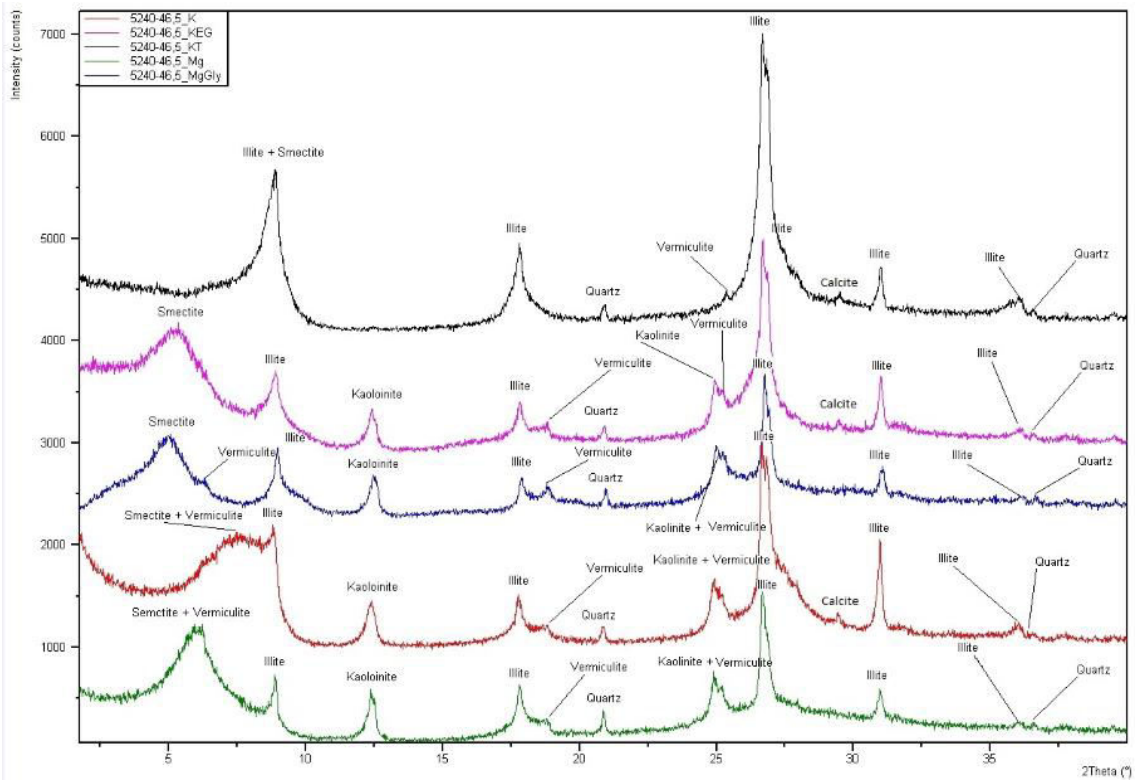

Figure 25: XRD patterns showing the clay mineralogy of sample 5240-46,5; Sarmatian

Table 4 shows the intensities of the main peaks for quartz (3.34 Å), calcite (3.03 Å), dolomite (2.88 Å) muscovite (10 Å) and pyrite (2.71 Å) in all bulk samples.

Table 4: Peak intensities for representative minerals (in counts)

Well	Depth (m)	Stratigraphic Stage	Qartz	Calcite	Dolomite	Muscovite	Pyrite
5240	18.45	Pannonian	9292	853.2	503.2	937.6	0
5240	21.9	Pannonian	8091.5	374.4	0	390.4	0
5240	22.6	Pannonian	20547.8	1261.1	0	91.8	0
5240	26.2	Pannonian	5089.9	988.6	741.6	425	0
5240	33.2	Pannonian	4750.6	721.9	689.8	336.1	0
5240	42.3	Pannonian	12609.7	1339.7	713.7	289.9	166.3
5240	45.6	Pannonian	19421.2	1360.2	559.9	183.9	213.5
5240	46.5	Sarmatian	5886.1	1186.9	1055.5	298.8	0
5240	58.2	Sarmatian	8012.2	1197.2	483.6	340.9	153.2
5260	26.5	Pannonian	7992.4	509.2	980.1	465.7	0
5260	32.2	Pannonian	6894.5	558.8	706.5	380.2	0
5260	37.8	Pannonian	5136.3	689.1	690.8	338.8	59
5260	42.4	Pannonian	5685	684.5	743.8	273.4	96
5260	52.5	Pannonian	9902.2	1262.9	615.8	346.9	99.5
5260	53.4	Sarmatian					
5260	53.9	Sarmatian	11097.3	1296.8	611.1	364.9	0
5260	59.8	Sarmatian	9380.4	1135.6	598.8	276	172.7

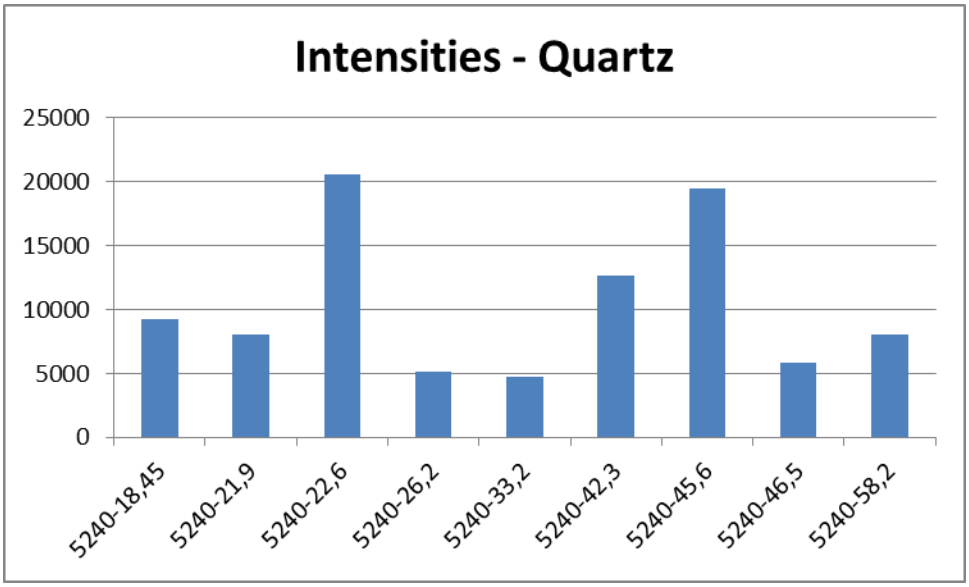

Figure 26: Peak intensities (counts) for quartz in well 5240

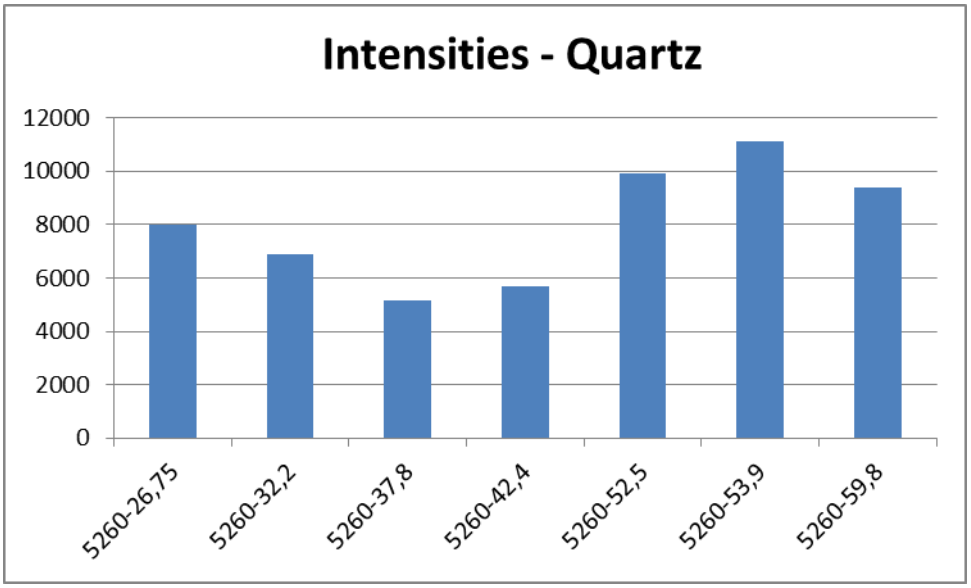

Figure 27: Peak intensities (counts) for quartz in well 5260

Figures 26 and 27 show that the coarser grained samples (5240-22,6, 5240-45,6 and the deepest 3 samples of well 5260) also have a higher content of quartz.

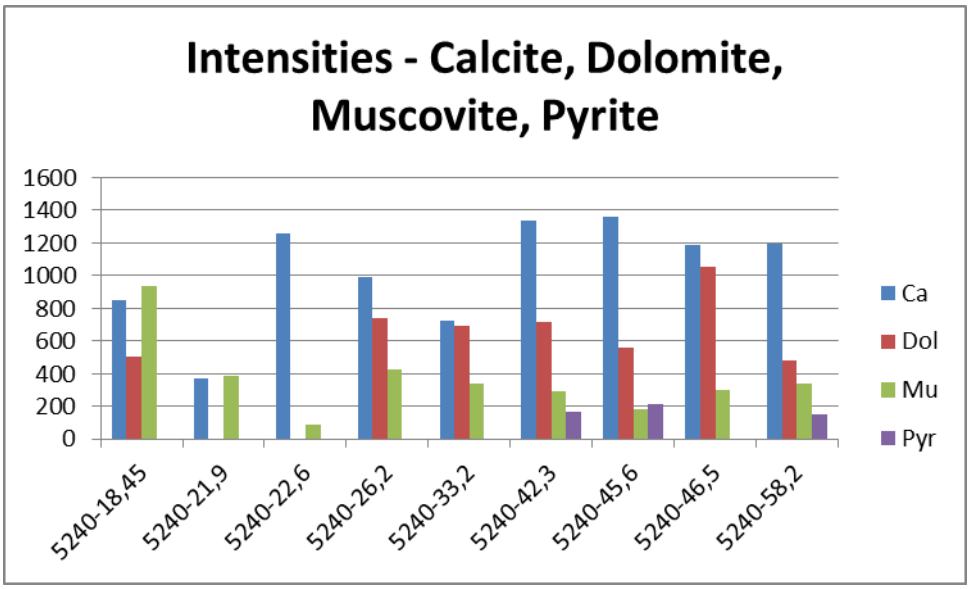

Figure 28: Peak intensities (counts) for calcite, dolomite, muscovite and pyrite in well 5240

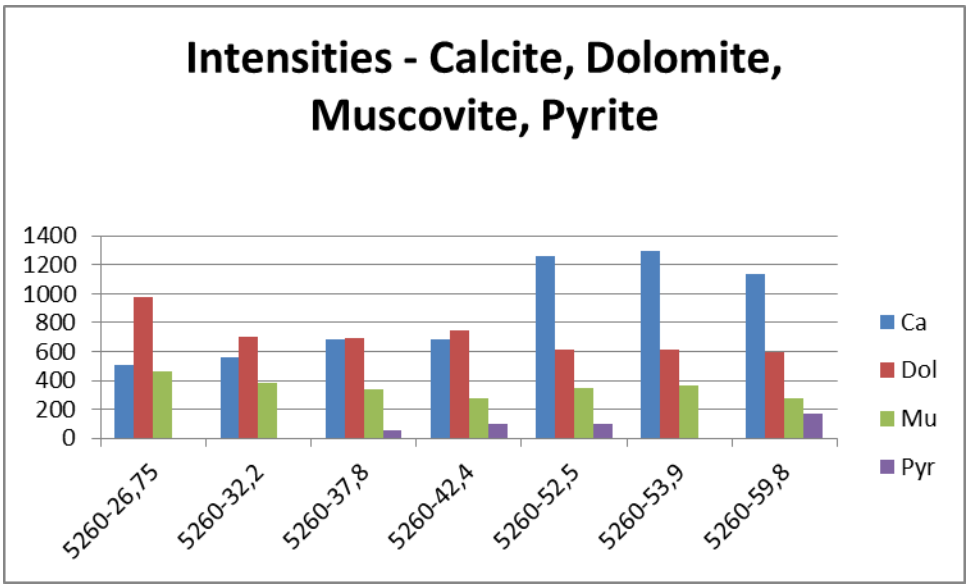

Figure 29: Peak intensities (counts) for calcite, dolomite, muscovite and pyrite in well 5260

The reddish samples (5240-21,9 and 5240- 22,6) do not contain dolomite (Figure 28). While intensities for muscovite stay quite constant, those for pyrite are present only for about half of the samples (Figures 28 and 29). Comparing the calcite intensities to the CaO content measured in the XRF spectroscopy (Table 3) shows that a big part of calcium is incorporated in calcite. The values increase generally with depth. The strong correlation between contents of SO_3 and pyrite as well as MgO and dolomite becomes obvious by comparing Figures 20 and 22 to Figures 28 and 29, respectively.

4.5 Carbonate Content

The two histograms (Figure 30 and 31) show the measured carbonate content in all the samples, except for the cobble/sand layer. Samples of the sandy layers have a significantly lower carbonate content than those from mudstones. The values also display a general increase in carbonate content with increasing depth. There is not any clear difference between Pannonian and Sarmatian sediments in general.

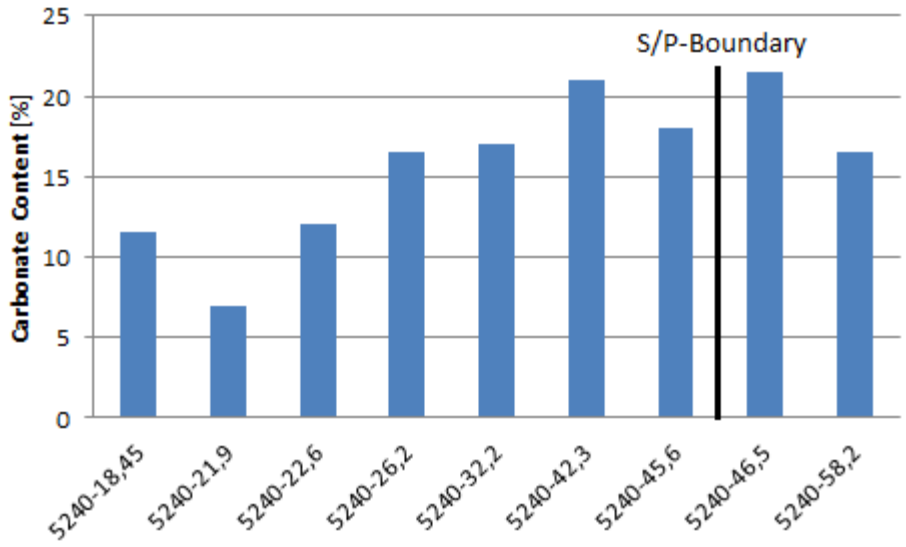

Figure 30: Carbonate content in well 5240

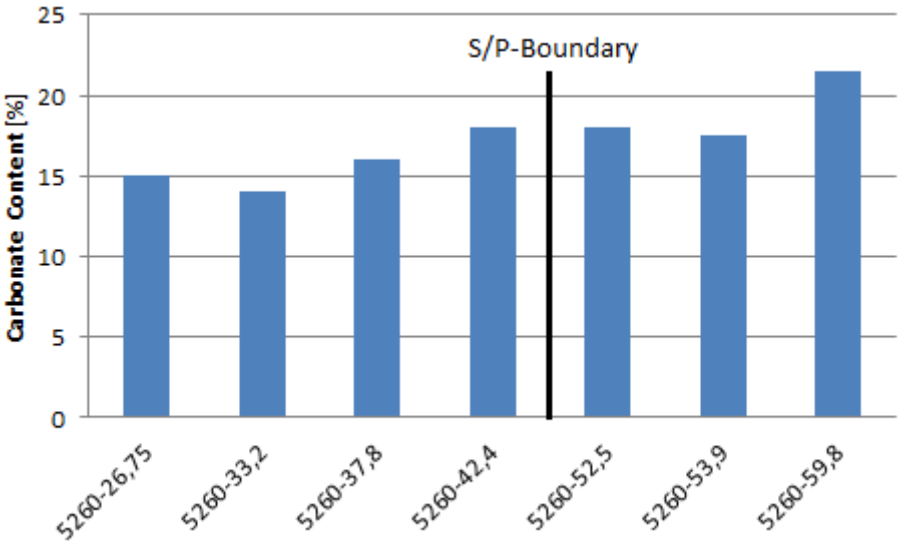

Figure 31: Carbonate content in well 5260

4.6 Total organic carbon measurement

The total organic carbon content gives a good hint to the predominant oxidizing regime. The lower the TOC value of a sample is, the higher the level of oxidation was in the sedimentation zone. Tissot and Welte (1984) present data for an average content of organic carbon in shales and mudstones of between 1 and 2.2 %. The two histograms below (Figure 32 and 33) show the content of organic carbon in all samples, except for the cobble/sand layer. The data showed a very low TOC content of below 1 % in all samples, which is, according to Hunt (1996), typical for green mudstones. The lowest values can be found in the oxidized reddish and brownish sands of the upper Pannonian of well 5240. There is no clear trend visible, neither between Pannonian and Sarmatian sediments nor in terms of depth.

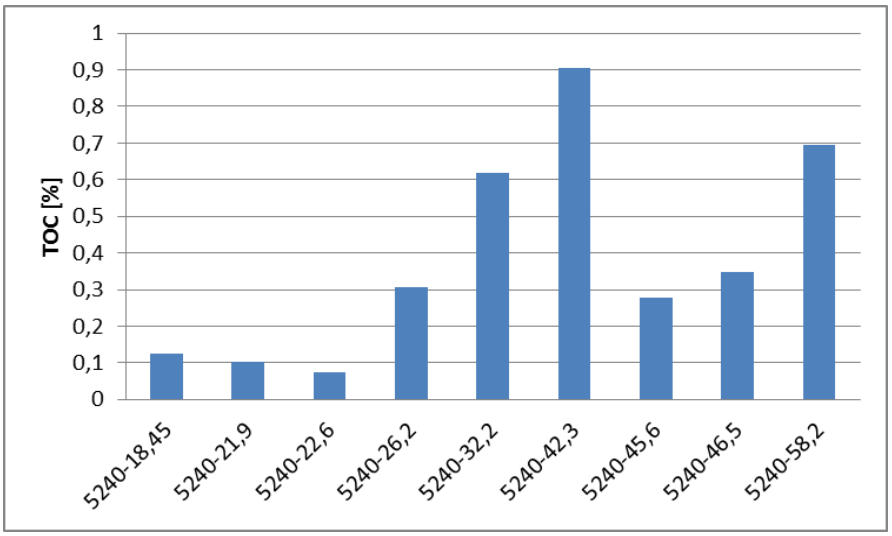

Figure 32: TOC values for samples of well 5240

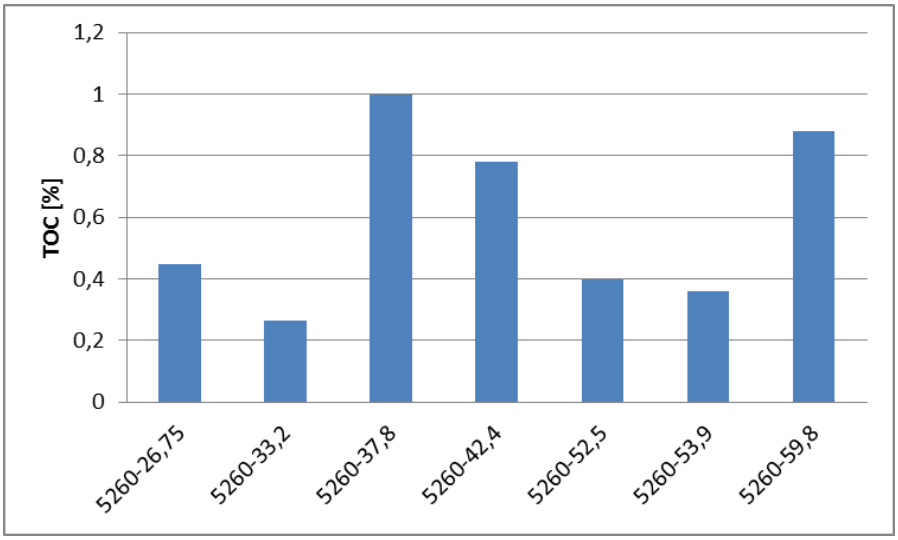

Figure 33: TOC values for samples of well 5260

4.7 Thin section microscopy

In order to clarify the provenance of the cobble/sand layer of well 5260 two samples of the cobble were taken, from which two thin sections were made in order to compare the texture and fossil content under the transmitted-light microscope to samples of the quaternary succession above the Miocene sediments. These quaternary layers have been described by Sophie Slawek (2015) in the course of her Bachelor's Thesis.

The thin sections made out of the two different types of cobble (53.0 until 53.5 m depth) display a different texture. The first type represents carbonatic sandstone. The texture is dominated by fine calcite grains embedded in a micritic matrix (Figure 34). Micro-fossils are abundant, e.g. planktonic foraminifera and sponge spicules (Figure 35).

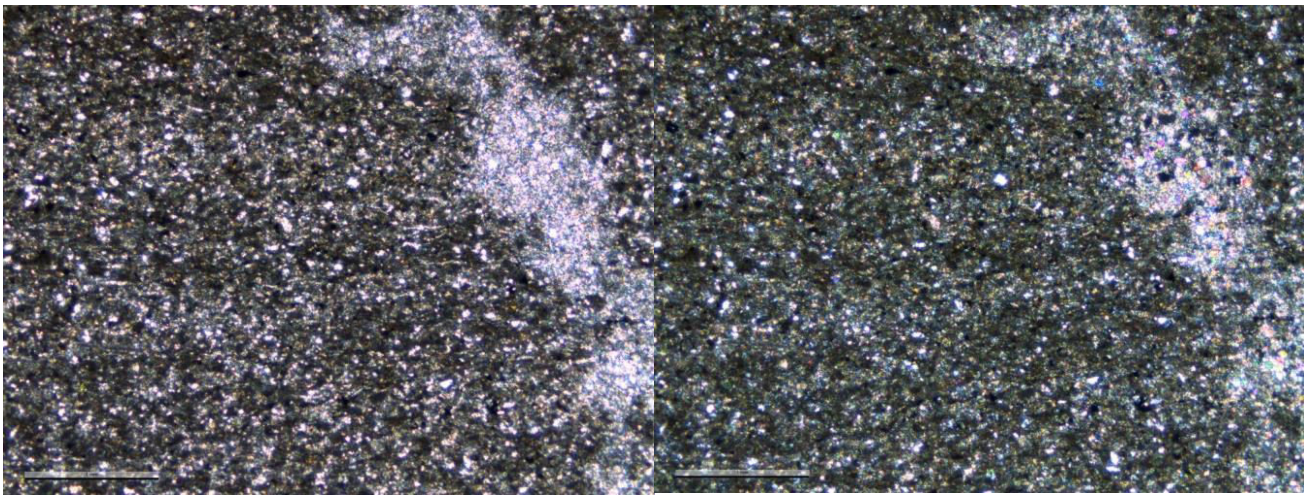

Figure 34: left: Photomicrograph of fine-grained carbonatic sandstone; plane-polarized light; right: Crossed polarized light; scalebar equals 1 mm

The second type represents a quartz-rich sandstone. Grains are coarser with an angular habitus

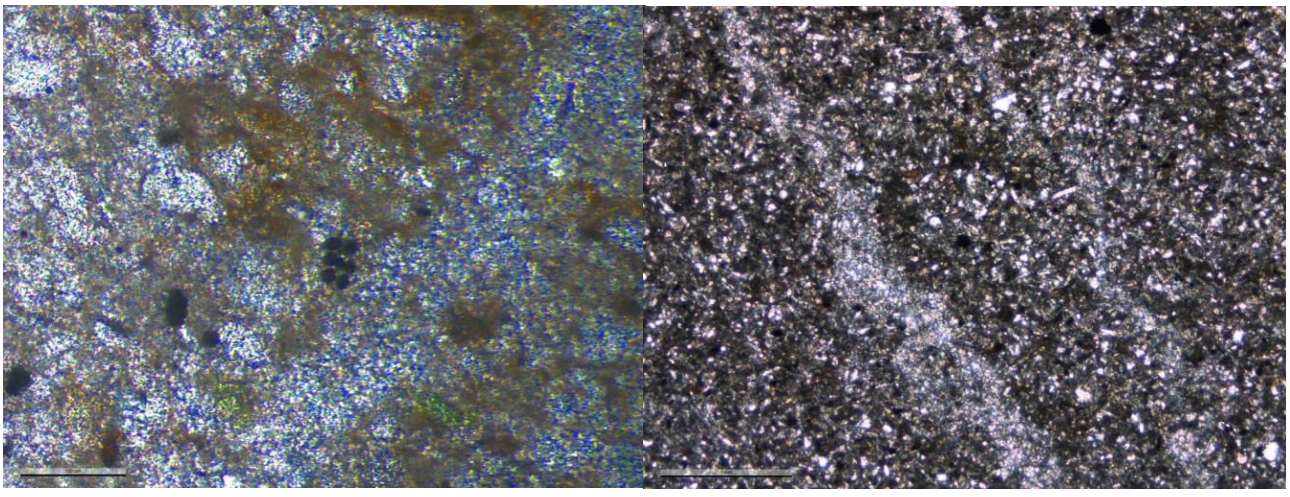

Figure 35: left: Photomicrograph of planktonic foraminifera in the centre, scalebar equals 100 µm; right: Photomicrograph of sponge spicules, scalebar equals 1 mm

(Figure 36), mostly consisting of quartz. The texture is grain supported without a matrix like in the carbonatic sandstones.

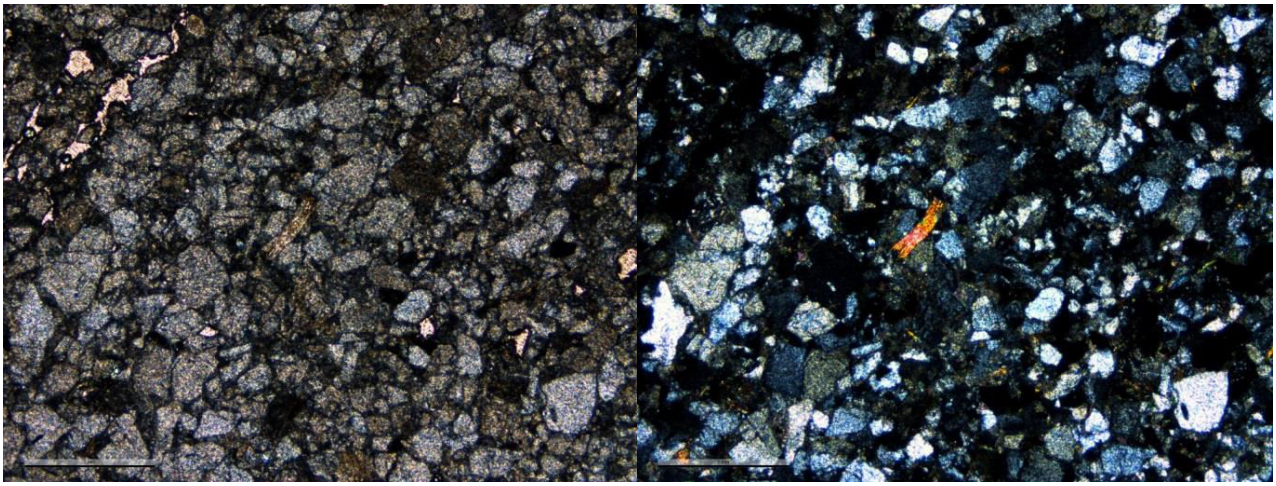

Figure 36: left: Photomicrograph of coarse-grained quartz – sandstone; plane-polarized light; right: crossed polarized light; scalebar equals 1 mm

5 Discussion

5.1 Colour Differences in Mudstones

One of the basic questions of this study was if there is a reason for the colour difference between Pannonian and Sarmatian sediments. The Pannonian sediments are of bluish-greyish colour, while the Sarmatian sediments have a more greenish-grey colour.

There are a variety of factors that can affect the colour of mudstones. One crucial factor is the degree of terrigenous dilution. Others are the flux of dissolved oxygen in the bottom- and pore waters as well as the influx of organic matter, which not least depends on ocean fertility (e.g. surface temperature) and the thickness of the well mixed water column above the bottom, where organic debris can get victim of consumption before it even settles down on the seafloor (Rothwell, 2005). Both have an impact on the colour of the resulting mudstone by affecting the oxidation state of iron, manganese and carbon. The amount of dissolved oxygen also affects the abundance of fossils, bioturbation and the amount of pyrite contained in the sediment (Hüneke and Mulder, 2011).

Grain size also matters, since finer grains reduce permeability and thus favour reduction leading to more intense colouring. High sedimentation rates, which equal quick burial of muds in a dysoxic or anoxic environment, generate predominantly red and gray colours (Potter et al., 2005). The amount of sulfate available in the bottom- and pore waters also plays a role in matters of colour, since sulfate triggers the oxidation of organic matter by bacteria after O_2 is completely consumed.

The provenance certainly also plays a big role. Fine grained material that comes along into the basin can contain greenish minerals like chlorite, glauconite and illite etc., but can also supply the mudstone with brown or red pigments. Furthermore, finely distributed pyrites are known for being responsible for the bluish colour in some mudstones (Potter et al., 2005).

Last but not least diagenesis can darken, discolour or bleach the former established colours after burial caused by oxidizing brines, hydrothermal solutions or heating by big close-by sills. Boggs (2006) argued that ferric iron (Fe^{3+}) that causes reddish colouring can be transformed to ferrous iron (Fe^{2+}) under reducing conditions during diagenesis, leading to a more greenish colour and vice versa.

There was basically no difference in bulk mineralogy or chemistry (e.g. pyrite- or TOC content) in the studied samples, which implies that there was neither a significant change in provenance nor in oxidation state of the sedimentary environment at the time of deposition or during diagenesis. There is also no evident difference concerning grain size, both Pannonian and Sarmatian sediments are dominated by clays- and silts.

Since all of the above described reasons suspected for causing the colour differences between the two stratigraphic units do not apply, the real reason remains unclear. A last attempt to explain the colour difference could be to link it to the different amount of fossils. The Sarmatian in the area of Vienna is known to possess a higher fossil content than the Pannonian. The higher amount of shell fragments in the Sarmatian sediments compared to those of the Pannonian could be seen in both cores (Figures 11 and 12). This high fossil abundance could possibly cause a macroscopic greenish effect.

5.2 Difference in Clay mineralogy

The x-ray patterns of the Pannonian and Sarmatian samples are very similar in terms of clay mineralogy (Figure 24 and 25). The following minerals could be detected in every sample: smectite (montmorillonite), vermiculite, illite, kaolinite and traces of chlorite, presumably clinochlore. Any differences in terms of clay mineralogy would also be a possible factor for colour differences, which will be discussed more detailed in the next chapter.

5.3 Brownish Weathering Crust

Both drilling cores feature a reddish-brownish crust at the top of the Pannonian, which varies greatly in thickness. Drilling core 5240 contains a 10 m thick brownish coloured sediment layer, whereas drilling core 5260 only has a 0.4 m thick one. The question was, why there is such a difference in thickness and whether this colouring is a matter of soil formation, weathering crust on the surface or subaqueous alteration. In order to clarify the genesis, data of grainsize, mineralogy, carbonate content, TOC and bulk chemistry have been compared (Figures 37 and 38).

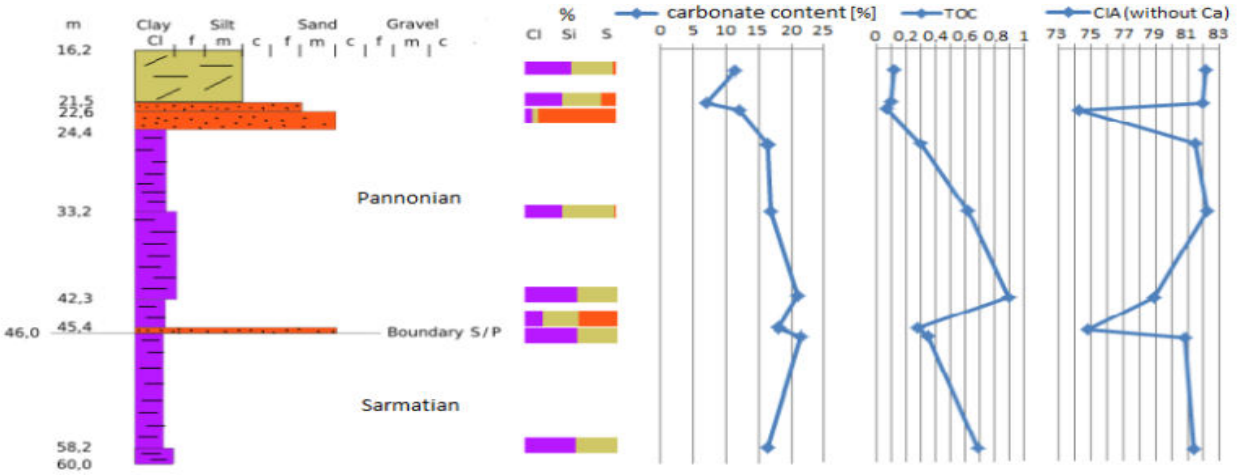

Figure 37: Lithostratigraphic profile of well 5240 compared to carbonate content, TOC and CIA (without Ca) with depth (Pannonian and Sarmatian)

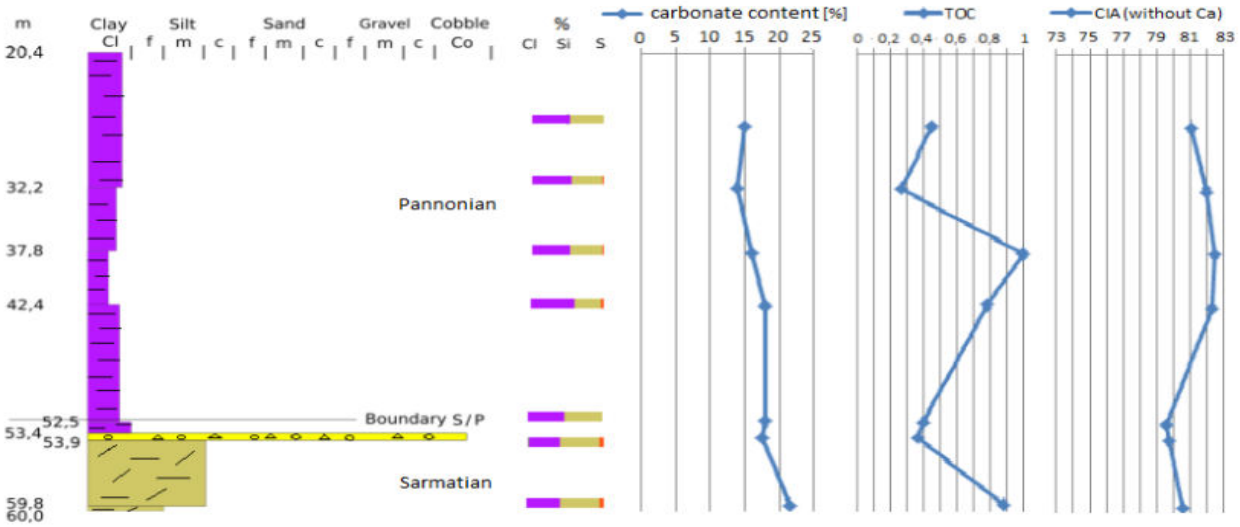

Figure 38: Lithostratigraphic profile of well 5260 compared to carbonate content, TOC and CIA (without Ca) with depth (Pannonian and Sarmatian)

Since the topmost sediments of the Pannonian in well 5240 mainly consist of material with silty and sandy grain size and possess a lower clay content (Figures 11 and 12, Table 2), the significant difference in thickness of the brownish weathering crust between wells 5240 and 5260 is most likely a function of grain size. Higher porosity allows better circulation of pore waters and leads to more oxic conditions on the seafloor. The brownish weathering crust is not a product of soil formation, but rather relates to subaqueous alteration, as no roots or plant imprints could be found inside the sediments. The low CIA value (Figures 17 and18) also argues against soil formation to be the originating process, since weathering in continental sedimentation conditions would cause a higher degree of chemical alteration.

Bland and Rolls (1998) argued that exposed rocks are constantly influenced by both physical and chemical weathering. While physical weathering ideally leads to a reduction in grain size but not to a change in mineralogical or geochemical features, continuous chemical weathering of chemically unstable minerals contained in exposed rocks generally results in a loss of Ca^{2+}, K^{+} and Na^{+}- ions (Fedo et al., 1995) and favors the transformation from feldspars to illite, kaolinite and Fe-oxyhydrates (e.g. goethite). Hydrolysis of silicate rocks induces an exchange of the Na^{+}-, K^{+}-, Ca^{2+}- and Mg^{2+}- for H^{+}-ions resulting in a relative increase in Al^{3+} in respect to those cations (Arnaud et al., 2009).

Since Na^{+}, K^{+} and Ca^{2+} can also be exchanged due to diagenetic processes as well, the impact of weathering on the geochemical content must be considered carefully when interpreting the CIA value (Wintsch and Kvale, 1994).

According to Andersson and Worden (2006) the degree of weathering is determined by the climate, i.e. humidity and to a lower level temperature, but also depends largely on the ground relief. Rocks originated from regions dominated by rapidly eroded mountains are characterized by less alterated chemisms than those located in flattened terrains which have undergone chemical weathering for a longer time period.

Because unweathered rocks have a similar CIA value to earth's average upper crust (McLennan et al., 1993) they come to around 45 – 55%. Potter et al. (2005) argue that values of between 70 and 80 % correspond best to those of illite and smectite. Kaolinite, gibbsite, chlorite and boehmite are more abundant in highly weathered sediments and have values of 100. The CIA values of the examined samples vary between 42.6 and 72.7, meaning that they are weathered to a lesser extent.

When looking at the results of the chemical analysis, one can clearly see the significant lower magnesium content in the reddish sands of sample 5240–22,6 (Figure 20). The lower MgO/Fe_2O_3 ratio in the brownish weathering crust of well 5240 is also a consequence of the coarser grainsizes and different mineralogy (Figures 39 and 40).

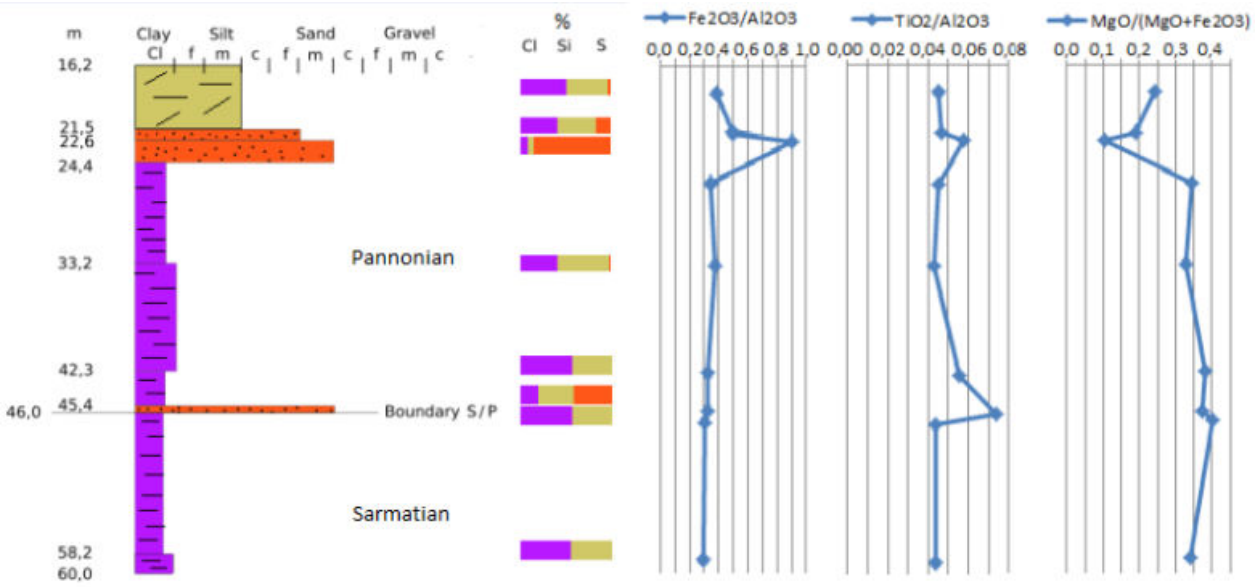

Figure 39: Lithostratigraphic profile of well 5240 compared to Fe_2O_3/Al_2O_3, TiO_2/Al_2O_3 and $MgO/(MgO/Fe_2O_3)$ wit depth (Pannonian and Sarmatian)

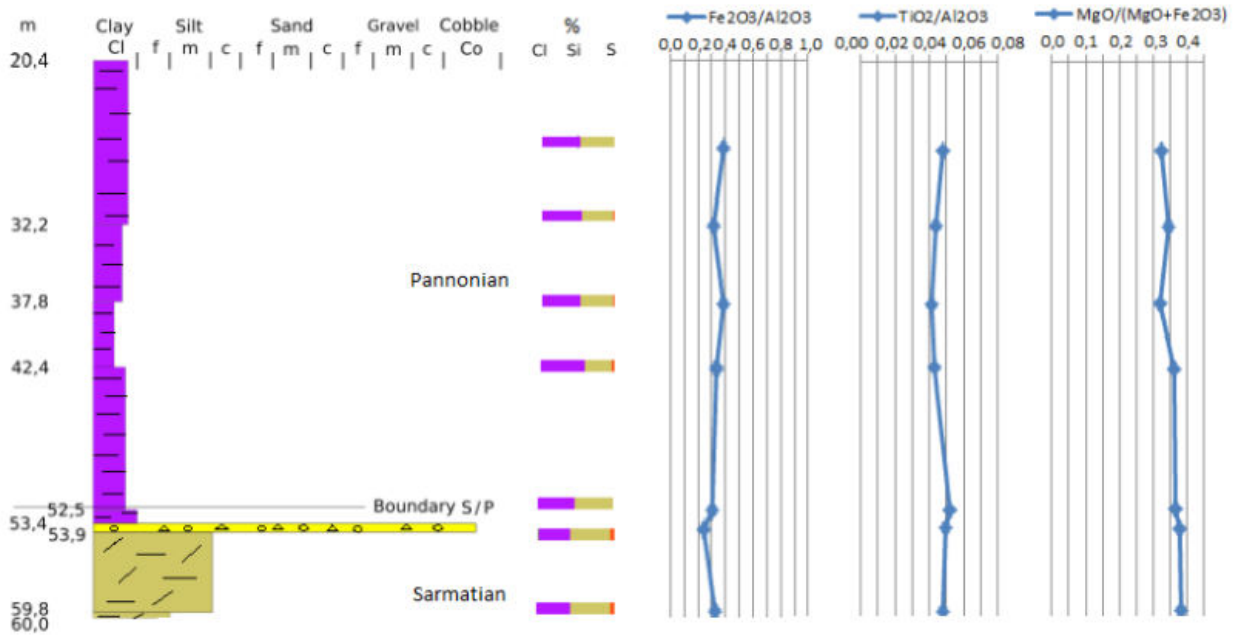

Figure 40: Lithostratigraphic profile of well 5260 compared to Fe_2O_3/Al_2O_3, TiO_2/Al_2O_3 and $MgO/(MgO/Fe_2O_3)$ wit depth (Pannonian and Sarmatian)

Comparing the x-ray patterns demonstrates that there is no dolomite, which is a main carrier of magnesium apart from various clay minerals. These two minerals probably were dissolved due to the high porosity, high oxidation state in the sediment and low pH value of pore waters. On the other hand sample 5240-22,6 contains a very high amount of quartz which is much more stable and better survives the solvation- and transport processes. A similar high abundance in quartz can only be seen in the sandy sample 5240-45,6, which shows that the amount of quartz is clearly linked to grainsize, since high porosity and acidic pore waters favour the dissolution of minerals like feldspars, but does not have a major effect on quartz. The oxidation of iron and manganese contained in the seafloor sediments results in reddish to brownish colouring. The higher amount of coarse grained material is believed to have derived from high-energy events like major storms.

The TiO_2/Al_2O_3 ratio gives a good hint for the provenance of a sediment (Andersson and Worden, 2004). The slightly higher TiO_2/Al_2O_3 ratio in sample 5240-22,6 an 5240-45,6 shown in Figures 39 and 40 is also due to a difference in grainsize and mineralogy and has nothing to do with a different provenance.

5.4 Provenance of the cobble/sand layer

The cobble/sand layer of well 5260 at a depth of approximately 53 m contains two different types of cobble, both resemble the two different types that occur in the Quaternary succession above the Miocene sediments, which have already been described by Slawek (2015) in the course of her bachelor's thesis. The first type, carbonatic sandstone (Figures 34 and 35), is similar to Quaternary carbonatic cobble/sandstone layer 16 – 19 m of core 5260. Comparison of the cobble of the second type (quartz-rich sandstone, Figure 36) to Quaternary sediments on top of the Miocene point out that these cobbles represent the same lithology as the cobble/sandstone layer at 20.1-20.5 m of drilling core 5260.
The provenance of the layer is believed to be the Flysch Zone, which is located north of the Eastern Alps, and could have been deposited during a high energy event.

6 Conclusions

The studied clays and sands of the two different wells display a generally quite homogenous geochemistry and (clay-) mineralogy, especially throughout the successions of well 5260. There were no clear differences between the Pannonian and Sarmatian sediments in terms of (clay-) mineralogy or chemistry, except for the topmost sediments of the Pannonian in well 5240. Since these sediments mainly consist of silty and sandy material with a lower clay content, the significant difference in thickness of the brownish weathering crust between wells 5240 and 5260 is most likely a function of grain size. These reddish and brownish colours are clearly linked to the coarser grain size that causes higher porosity and therefore allows pore waters and fluids to better migrate through the sediment and oxidize iron and manganese. The presence of this layer of coarser grained material is most likely the result of a high energy event. This might also be the reason for the cobble/sand layer corresponding to sample 5260-53,4, which contains cobbles, most likely originating from the Flyschzone, that are lithological identical to the ones of the Quaternary sediments above described by Slawek (2015).

The brownish sediments neither contain any remains of plants or roots nor any imprints, and the low CIA value also argues against soil formation and favours subaqueous alteration.

Although many different possible reasons for colour changes in mudstones have been taken in consideration, the real cause for the colour difference between Pannonian and Sarmatian sediments could not be established. The reason for the more greenish colours of Sarmatian clays compared to the more bluish ones of the Pannonian is most likely a macroscopic effect caused by a general higher fossil content in sediments of the Sarmatian.

7 References

Andersson, P.O.D. and Worden, R.H. 2004. Mudstones of the Tanqua Basin, South Africa: an analysis of lateral and stratigraphic variations within mudstones, and a comparison of mudstones within and between turbidite fans. Sedimentology. Vol. 51, Issue 3, pp. 479-502

Andersson P.O.D. and Worden R.H. 2006. Stratigraphic variations in mudstone mineral assemblages from a submarine fan-complex: Karoo Basin, South Africa. Clay Minerals 41, pp. 839-852

Arnaud, E., Halverson, G.P. and Shields, G.A. 2009. A review of the Chemical Index of Alteration (CIA) and its application to the study of Neoproterozoic glacial deposits and climate transitions. The Geological Record of Neoproterozoic Glaciations. Geological Society, London, Memoir. pp. 3-15

Bland, W. and Rolls, D. 1998. Weathering. An introduction to the scientific principles. Arnold Publishers, London. pp. 271

Boggs, S. Jr. 2006. Petrology of Sedimentary Rocks. Cambridge University Press, New York. pp. 206-215

Chesworth, W. 2008. Encyclopedia of Soil Science. University of Guelph. Canada. Springer. p. 510

Fedo, C.M., Nesbitt, H.W. and Young, G.M. 1995. Unraveling the effects of potassium metasomatism in sedimentary rocks and paleosols, with implications for paleoweathering conditions and provenance. Geology 23, p. 921-924.

Hunt, J. M. 1996. Petroleum Geochemistry and Geology. 2nd edn. W. H. Freeman, New York. Table 10-1

Hüneke, H., and T. Mulder (2011) Deep-Sea Sediments. Developments in Sedimentology. vol. 63. Elsiever, Amsterdam. pp. 849

Jasmund, K. and Lagaly, G. 1993. Tonminerale und Tone - Struktur, Eigenschaften, Anwendungen und Einsatz in Industrie und Umwelt. Steinkopff Verlag Darmstadt. pp. 13-28

Kováč, M., Baráth, I., Harzhauser, M., Hlavatý, I., Hudáčková, N. 2004. Miocene depositional systems and sequence stratigraphy of the Vienna Basin. Cour. Forsch.-Inst. Senckenberg. p. 197

McLennan, S.M., Hemming, S., McDaniel, D. K. and Hanson, G.N. 1993. Geochemical approaches to sedimentation, provenance, and tectonics. Geological Society of America Special Papers.

Müller, G. and Gastner, M. 1971. The 'Karbonat-Bombe', a simple device for the determination of carbonate content in sediment, soils, and other materials. Neues Jahrbuch für Mineralogie-Monatshefte, Bremerhaven, PANGAEA, 10 , pp. 466-469.

Nesbitt, H.W., Young, G.M. 1982. Prediction of some weathering trends of plutonic and volcanic rocks based on thermodynamic and kinetic considerations. J Geol 48, pp. 1523-1534

Picard, M. D. 1971. Classification of fine-grained sedimentary rocks. J. Sediment Petrol. , 41, p. 185. Fig. 3

Pisera, A. 1996. Miocene reefs of the Paratethys: A review. SEPM Concepts in Sedimentology and Paleontology. SEPM, Soc. Sed. Geol., 5. pp. 97-104

Potter, P.E., Maynard, J.B. and Depetris, P.J. 2005. Mud and Mudstones: Introduction and Overview. Springer-Verlag Berlin Heidelberg. p. 13, pp. 66-72

Rees, H. 1974. Italy, Switzerland and Austria: a geographical study. London.

Reitner, J.M. 2013. Quartärgeologie SS 2013, Unterlagen zur Vorlesung. p. 32

Rögl, F. 1999. Mediterranean and Paratethys. Facts and Hypotheses of an Oligocene to Miocene Paleography (Short Overview). Geologica Carpathica, 50, 4, Bratislava. p. 348

Rothwell, R.G. 2005 Deep Ocean Pelagic Oozes. In: Selley, R. C., L. R.
McCocks, and I. R. Plimer (eds.), Encyclopedia of Geology Vol. 5, Oxford: Elsevier Limited.

Royden, L. H. 1985. The Vienna Basin: a thin-skinned pull-apart basin. In: Biddle, K. T. & Christie-Blick, N. (eds.) Strike-Slip Deformation, Basin Formation and Sedimentation. Society of Economic Paleontologists and Mineralogists (SEPM), Special Publications, 37, pp. 319–339

Sachsenhofer, R. F. 2001. Syn- and post-collisional heat flow in the Cenozoic Eastern Alps. International Journal of Earth Sciences 90, pp. 579–592

Seifert, P. 1996. Sedimentary–tectonic development and Austrian hydrocarbon potential of the Vienna Basin. In: Wessely, G. & Liebl, W. Oil and Gas in Alpidic Thrustbelts and Basins of Central and Eastern Europe. European Association of Geoscientists & Engineers (EAGE), Special Publications, 5, p. 331–341

Slawek, S. 2015. Quartäre Terrassen in Wien: Sedimentpetrologische Untersuchungen an Bohrkernen (Umgebung AKH). Unpublished BSc thesis. Universität Wien. pp. 19-37

Strauss, P. 2006. Badenian paleoenvironment of the Vienna Basin. Geologica Carpathica 57, 3, p. 188

Tissot, B.P. and Welte, D.H. 1984. Petroleum Formation and Occurrence. Springer-Verlag Berlin Heidelberg. p. 97

Wintsch, R.P. and Kvale, C.M. 1994. Differential mobile ty of elements in burial diagenesis of siliciclastic rocks. Journal of Sedimentary Research A64. pp. 349–361

Wagreich, M. and Schmid, H. P. 2002. Backstripping dipslip fault histories: apparent slip rates for the Miocene of the Vienna Basin. Terra Nova, 14, p. 163–168

Wien.at, Probebohrungen für U5 und U2, [Online],
Available: https://www.wien.gv.at/verkehr/grundbau/baustellen/probebohrungen.html
[07 Aug 2016].

Wien.at, U-Bahn-Ausbau U2 und U5, [Online],
Available: https://www.wien.gv.at/stadtentwicklung/projekte/verkehrsplanung/u-bahn/u2u5/
[14 Apr 2016].

Wien.at, Verkehr – Stadtentwicklung - Fahrplan, [Online],
Available: https://www.wien.gv.at/verkehr-stadtentwicklung/fahrplan/oeffi-paket.html
[14 Apr 2016].